Manuscript no. 2027

The number of synaptic inputs and the synchrony of large sparse neuronal networks

D. Golomb [1] and D. Hansel [2]

[1] *Zlotowski Center for Neuroscience and Dept. of Physiology, Faculty of Health Sciences*

Ben Gurion University of the Negev, Be'er-Sheva 84105, Israel

[2] *Laboratoire de Neurophysique et de Physiologie du Système Moteur*

EP 1848 CNRS, Université René Descartes

45 rue des Saints Pères, 75270 Paris Cedex 06, France

Running title: Synchrony of sparse networks

Keywords: Synchronization, sparseness, phase reduction, inhibition, weak coupling, cluster states

Abstract

The prevalence of coherent oscillations in various frequency ranges in the central nervous system raises the question of the mechanisms that synchronize large populations of neurons. We study synchronization in models of large networks of spiking neurons with random sparse connectivity. Synchrony occurs only when the average number of synapses, M, that a cell receives is larger than a critical value, M_c. Below M_c, the system is in an asynchronous state. In the limit of weak coupling, assuming identical neurons, we reduce the model to a system of phase oscillators which are coupled via an effective interaction, Γ. In this framework, we develop an approximate theory for sparse networks of identical neurons to estimate M_c analytically from the Fourier coefficients of Γ. Our approach relies on the assumption that the dynamics of a neuron depend mainly on the number of cells that are presynaptic to it. We apply this theory to compute M_c for a model of inhibitory networks of integrate-and-fire (I&F) neurons as a function of the intrinsic neuronal properties (*e.g.,* the refractory period T_r), the synaptic time constants and the strength of the external stimulus, I_{ext}. The number M_c is found to be non-monotonous with the strength of I_{ext}. For $T_r = 0$, we estimate the minimum value of M_c over all the parameters of the model to be 363.8. Above M_c, the neurons tend to fire in: 1) smeared one cluster states at high firing rates and 2) smeared two or more cluster states at low firing rates. Refractoriness decreases M_c at intermediate and high firing rates. These results are compared against numerical simulations. We show numerically that systems with different sizes, N, behave in the same way provided the connectivity, M, is such a way that $1/M_{\text{eff}} = 1/M - 1/N$ remains constant when N varies. This allows one to extrapolate the large N behavior of a network from numerical simulations of networks of relatively small sizes ($N = 800$ in our case). We find that our theory predicts with remarkable accuracy the value of M_c and the patterns of synchrony above M_c, provided the synaptic coupling is not too large. We also study the strong coupling regime of inhibitory sparse networks. All of our simulations demonstrate that increasing the coupling strength reduces the level of synchrony of the neuronal activity. Above a critical coupling strength, the network activity is asynchronous. We point out that there is a fundamental limitation for the mechanisms of synchrony relying on inhibition alone, if heterogeneities in the intrinsic properties of the neurons and spatial fluctuations in the external input are also taken into account.

1 Introduction

The ubiquity of coherent oscillations in the central nervous system (for a review see Gray 1994), raises fundamental biophysical issues concerning the role of intrinsic neuronal and synaptic characteristics in the emergence of coherent neuronal activity. In recent years, these issues have been addressed in various theoretical studies focusing mostly on the simplest situation in which the neurons are identical and coupled all-to-all (Gerstner 1999, Gerstner *et al.* 1996, Hansel *et al.* 1993a,b,c, 1995, van Vreeswijk *et al.* 1994). These studies have demonstrated that the degree of synchrony which can emerge in a large neural system depends crucially on the nature, whether excitatory or inhibitory, of the synaptic interactions between the neurons. More recently, the effect of heterogeneities in neuron properties, still assuming an all-to-all coupling (Chow 1998, Chow *et al.* 1998, Neltner *et al.* 1999, White *et al.* 1998) have been investigated. On the basis of these studies, it has been suggested that inhibition should play a crucial role in the emergence of synchrony in the central nervous system. Similar conclusion has been reached, in parallel with these theoretical investigations, in experimental studies in *in vitro* preparations. Indeed, Whittington *et al.* (1995) demonstrated that an inhibitory population can fire in synchrony in the gamma band even if the excitatory population is blocked pharmacologically. This result goes along the idea that pyramidal cells *in vivo* may be entrained by synchronous rhythmic inhibition originating from fast spiking interneurons, as suggested as early as 1983 by Buszaki *et al.* (Buzsáki *et al.* 1983, Buzsáki and Chrobak 1995; see also the theoretical study by Lytton and Sejnowski 1991, and by Tiesinga and Jose 1999).

As mentioned above, most of the theoretical investigations of neural synchrony in large networks have focused on all-to-all architecture. However, in cortex, each neuron is coupled to only a certain number of neurons which is much smaller than the total number of neurons in the network. This property of the network architecture, referred to as "sparseness" or "dilution", is expected to reduce, or even destroy, the synchrony in the network even if the corresponding network with all-to-all coupling is highly coherent. It is often assumed in models that the coupling between neurons is random. In these cases (Barkai *et al.* 1990, Wang *et al.* 1995), it was found that when the all-to-all network is synchronized, synchrony will still prevail if the average number of inputs a cell receives is larger than a critical number. Wang and Buzsáki (1996) numerically studied a model of a sparse and heterogeneous network made of spiking neurons with inhibitory coupling. They claimed that synchrony could emerge if the ratio between the synaptic decay time constant and the

oscillation period was sufficiently large and the heterogeneity level was modest. For their specific parameter set, they obtained that the average number of input a cell should receive in order to get synchrony is on the order of 100. However, one expects this number to depend on the intrinsic properties of the cells as well as on the synaptic and network properties.

In this paper, we study models of large sparse networks made of identical intrinsically-oscillating neurons with inhibitory coupling. Our goal is to find how the critical average number of synaptic inputs, M_c, above which synchrony emerges, and the patterns of synchrony in networks in which neurons receive more inputs than this critical number depend on the intrinsic and synaptic properties of the neurons. Our strategy is to study the limit of weak synaptic coupling in which the network dynamics can be reduced to the dynamics of coupled phase oscillator which, to a large extent, can then be studied analytically. Using an approximate mean-field theory, we estimate the critical average number of inputs for the integrate-and-fire ($I\&F$) neuron model. This result helps us to understand the network dynamics even beyond this limit, as obtained numerically. Simulations of sparse $I\&F$ networks are performed to verify the prediction of our approximate theory for finite (but not too strong) coupling, to find the patterns of synchrony in networks for which the asynchronous state is unstable, and to study the model behavior beyond the weak coupling limit.

The paper is organized as follows: In the next section we present a general framework for modeling diluted networks. Section 3 is devoted to the weak coupling case. The theory is applied to networks of $I\&F$ neurons in Section 4, and simulations of such networks are described in Section 5. Section 6 summarizes and discusses our findings.

2 The model

2.1 Architecture of the network

We are interested in the dynamics of one population of N neurons of the same type, i.e., all excitatory or all inhibitory, which are randomly connected. A neuron, $i, (i = 1, \ldots, N)$ is making one synapse on neuron j with a probability M/N, where $M < N$. We define a connectivity matrix w_{ij} by:

$$w_{ij} = \begin{cases} 1 & \text{if neuron } j \text{ is presynaptic to neuron } i \\ 0 & \text{otherwise} \end{cases} \tag{2.1}$$

In this architecture, the number of synaptic inputs fluctuates from neuron to neuron with a population average M. The total synaptic input received by neuron i is:

$$g_{\mathrm{syn},i}^{\mathrm{tot}} = \frac{g_{\mathrm{syn}}}{M} \sum_{j=1}^{N} w_{ij} s_j \tag{2.2}$$

where s_i is the synaptic variable of the ith neuron and g_{syn} does not depend on M. With this normalization, the system-average synaptic input which a cell receives when all of the synaptic channels are open ($s_i = 1$ for all i) is g_{syn}. The standard deviation of the neuron-to-neuron fluctuations is

$$g_{\mathrm{syn}} \sqrt{\frac{1}{M} - \frac{1}{N}} \tag{2.3}$$

This value is equal to $g_{\mathrm{syn}}/\sqrt{M}$ for $N >> M$. The spatial fluctuations in the synaptic input decrease as M increases, and we expect the system to be more synchronized. Analysis of diluted networks is often carried out in two behavioral regimes:

1. The ratio M/N remains constant as $N \to \infty$. In this regime, input fluctuations go to zero at large N, and the behavior is similar to the case of all-to-all coupling ($M = N$) (Golomb *et al.* 1994).

2. The number M remains constant as $N \to \infty$. This is the *sparse* regime, and synchrony is expected to be reduced at small values of M in comparison to the case $M = N$. In previous work on different systems (Barkai *et al.* 1990, Wang *et al.* 1995, Wang and Buzsáki 1996), it was suggested that the asynchronous state is stable if M is below a critical value M_c.

In this work we study the dynamical properties of sparse networks in the limit $N \to \infty$.

2.2 Integrate-and-fire dynamics

In this paper we will mainly study networks of $I\&F$ neurons (Tuckwell, 1988, Abbott and van Vreeswijk 1993, Bressloff and Coombes 1998a,b, Brunel and Hakim 1999, Chow 1998, Gerstner 1999, Gerstner *et al.* 1996, Hansel *et al.* 1995, Kuramoto 1991, Mirollo and Strogatz 1990, Treves 1993, Tsodyks *et al.* 1993, Tsodyks and Sejnowki 1995, van Vreeswijk *et al.* 1994). This enables us to investigate the synchronization properties of models without active ionic currents that generate spikes. In the following, we study the simplest $I\&F$ model (the Lapicque model) in which the membrane potential of a neuron satisfies the differential equation:

$$\frac{dV}{dt} = -\frac{V}{\tau_0} + I_{\mathrm{ext}} + I_{\mathrm{syn}}(t) \tag{2.4}$$

for $0 < V < \theta$ and

$$V(t_0^+) = 0 \quad \text{if} \quad V(t_0^-) = \theta \tag{2.5}$$

This last condition corresponds to a fast resetting of the neuron after the firing of a spike at time t_0; this firing occurs when the membrane potential reaches the spiking threshold θ; we choose $\theta = 10$ mV above rest. The time constant of the membrane is $\tau_0 = 10$ ms and $I_{\rm ext} = \tilde{I}_{I_{\rm ext}}/C$, where $\tilde{I}_{I_{\rm ext}}$ represents the contribution of an external (e.g., sensory) stimulus to the system. The quantity, C, is the membrane capacitance. Note that the normalized parameter, $I_{\rm ext}$, has units of $\mathrm{mV/ms}$.

Refractoriness is introduced into the model by imposing that $V(t)$ remains equal to 0 for a refractory period, T_r, after the firing of a spike. The last term in Eq. 2.4 is the synaptic current received by the neuron, normalized to the value of C. For this model we adopt:

$$I_{\rm syn}(t) = g_{\rm syn}\, s\,(t) \tag{2.6}$$

where $g_{\rm syn}$ is the normalized synaptic current (in units of mV/ms) and s is a synaptic variable given by

$$s = \sum_{\rm spikes} f(t - t_{\rm spike}) \tag{2.7}$$

where the summation is done over all of the spikes emitted prior to t by all of the neurons presynaptic to the neuron we consider. With this simplified form of synaptic coupling, excitation corresponds to $g_{\rm syn} > 0$ and inhibition to $g_{\rm syn} < 0$. The function, $f(t)$, is the extended α-function:

$$f(t) = \frac{\exp\left(-t/\tau_2\right) - \exp\left(-t/\tau_1\right)}{\tau_2 - \tau_1} \tag{2.8}$$

The characteristic times τ_1 and τ_2 are the rise and decay times of the synapse respectively; $\tau_1 \leq \tau_2$. If the neurons are not interacting ($g_{\rm syn} = 0$) they emit spikes periodically for $I_{\rm ext} > \theta/\tau_0$ with a firing period, T_0 (firing frequency $f_0 = 1/T_0$)

$$T_0 = T_r - \tau_0 \ln\left(1 - \frac{\theta}{\tau_0\, I_{\rm ext}}\right) \tag{2.9}$$

3 The weak coupling limit

3.1 Reduction to phase models

In general, the dynamical equations of large networks of spiking neurons cannot be solved analytically, and the study of synchronization in such networks relies on numerical computations.

However, under the following three conditions the state of each neuron can be described by a phase variable, ϕ_i, which characterizes at time t, the location of neuron i along its limit cycle (Kuramoto, 1984).

1. The uncoupled neurons display a periodic behavior (limit cycle) when the external current is above some threshold;

2. Their firing rates all lie in a narrow range, i.e, the heterogeneities in the neuronal intrinsic properties and in the external inputs are small;

3. The coupling is weak (and therefore it modifies the firing rate of the neurons only slightly).

The original system of equations for the N oscillators are replaced by a simpler set of N differential equations that governs the time evolution of the ϕ_i:

$$\frac{d\phi_i}{dt} = 2\pi f_{0i} + \frac{1}{M}\sum_{j\neq i} w_{ij}\Gamma\left(\phi_i - \phi_j\right) \tag{3.1}$$

where f_{0i} is the firing rate of neuron i, when uncoupled. Here, Γ is the effective interaction between any two neurons:

$$\Gamma\left(\phi_i - \phi_j\right) = \frac{1}{2\pi}\int_0^{2\pi} Z\left(\psi + \phi_i\right) I_{\rm syn}\left(\psi + \phi_i, \psi + \phi_j\right)\, d\psi \tag{3.2}$$

The function Z is the phase resetting curve (Kuramoto 1984, Hansel et al. 1993a) of the neuron in the limit of vanishingly small perturbations of the membrane potential, and $I_{\rm syn}(\phi_i, \phi_j)$ is the synaptic interaction which is a function of the phases of the pre-synaptic and postsynaptic neurons. The function Γ depends only on the single neuron dynamics. For simple $I\&F$ neurons it can be computed analytically. For conductance-based neuronal models, numerical methods have to be used as described in Ermentrout and Kopell (1984), Kopell (1988), or in Hansel *et al.* (1993a.) Once this effective phase interaction is determined, it can be used to analyze networks of arbitrary complexity.

Reduction to a phase model assumes that the coupling is small enough for amplitude effects to be neglected. The more stable the limit cycle, the weaker this constraint will be, but it is difficult to derive quantitative a priori estimates of the validity of the phase reduction. However, predictions of phase models often remain valid, at least qualitatively, for moderate values of the coupling. This is the case for the examples studied below.

3.2 Approximate theory for randomly and weakly coupled neurons

The Fourier series representation of the Γ function is:

$$\Gamma(\phi) = \Gamma_0 + \tilde{\Gamma}(\phi) = \Gamma_0 - |\Gamma_0| \sum_{n=1}^{\infty} c_n \sin(n\phi + \alpha_n) \tag{3.3}$$

where Γ_0 is the zeroth Fourier component of $\Gamma(\phi)$, $\tilde{\Gamma}(\phi)$ includes all the phasic components of Γ, c_n is the normalized amplitude of the nth Fourier component and is therefore always non-negative, and α_n is the angle of that mode. This parameterization is chosen in order to be consistent with previous works on networks of phase oscillators (Kuramoto, 1984; Strogatz and Mirollo, 1991).

Substituting Eq. 3.3 in Eq. 3.1 yields the following dynamics

$$\frac{d\phi_i}{dt} = 2\pi f_{0i} + \frac{m_i \Gamma_0}{M} + \frac{1}{M} \sum_{j=1}^{N} w_{ij} \tilde{\Gamma}(\phi_i - \phi_j) \quad i = 1, ..., N \tag{3.4}$$

where

$$m_i = \sum_{j=1}^{N} w_{ij} \tag{3.5}$$

is the number of synaptic inputs the ith cell receives from other cells. The second term in this equation is a major source of disorder in the system which tends to desynchronize it. For example, if $\Gamma_0 < 0$, a cell that receives a larger number of inputs, m_i, will tend, in general, to delay the time of occurrence of its next spike in comparison to another cell that receives a smaller m_i. The third term in Eq. 3.4 includes the Fourier components which depend on the difference $\phi_i - \phi_j$ and therefore can help to synchronize the system. Therefore, the synchronization of the system is determined by a competition between the second and third terms.

In most of the paper we assume that all the neurons are identical, *i.e.,* $f_{0i} = f_0$ for $i = 1, ...N$. In that case the first term in Eq. 3.4 can be gauged out of the equations. We analyze the synchronization properties of Eq. 3.4 in the limits

$$N \to \infty \tag{3.6}$$

and

$$1 \ll M \ll N \tag{3.7}$$

The number of neurons that receive m inputs is a binomial distribution that we denote by $P_0(m, M)$. Under the condition $N \gg M \gg 1$ (3.7), this distribution (Eqs. 2.1,3.5) becomes a Gaussian distribution, $P(\delta m, M)$:

$$P\left(\delta m, M\right) = \frac{1}{\sqrt{2\pi M}} \exp\left(\frac{-\delta m^2}{2M}\right) \tag{3.8}$$

where $\delta m = m - M$. In this work, we develop an approximate theory. Our analysis is based on the assumption that the state of the network at time t can be characterized by the density function $\rho\left(\phi, t, \delta m\right)\, d\phi$ which is the fraction of neurons with $M + \delta m$ inputs whose phase lies between ϕ and $\phi + d\phi$ at time t. It is normalized such that

$$\int_{-\pi}^{\pi} \rho\left(\phi, t, \delta m\right)\, d\phi = 1 \tag{3.9}$$

In other words, we assume that the dynamics of a neuron depends only on the number of inputs it directly receives from other neurons in the network and we derive (approximate) dynamics in terms of a Fokker-Planck equation for ρ (Eq. (A1)). As shown in Appendix A, this amounts to the assumption that most of the effects of the sparseness is due to the second term in Eq. 3.4. This is exact in the limit $c_n \to 0$ for all n, but only approximate for a general phase model (Golomb and Hansel, unpublished). However, as we will see below, this approximation provides good estimates in the case of neuronal systems.

The asynchronous state is given by

$$\rho_0\left(\phi, t, \delta m\right) = \frac{1}{2\pi} \tag{3.10}$$

In Appendix A we estimate the critical value, M_c, such that for $M > M_c$ the asynchronous state is an unstable solution of the (approximate) dynamics. Here we give the final results. The critical number, M_c, is the minimum of the numbers, $M_{c,n}$, over all positive integers, n, for which it is finite:

$$M_c = \min_n M_{c,n} \tag{3.11}$$

where $M_{c,n}$ is determined by the amplitude, c_n, and the phase, α_n, of the nth Fourier term of $\Gamma\left(\phi\right)$ (Eq. 3.3)

$$M_{c,n} = \begin{cases} 8/\left[\pi c_n^2 \beta^2\left(\alpha_n\right)\right] & -\pi/2 < \alpha_n < \pi/2 \\ \text{infinity} & \text{otherwise} \end{cases} \tag{3.12}$$

The function $\beta(\alpha)$ is universal and does not depend on the model details (see Fig. 12B). It is a decreasing function of $|\alpha|$. As $\alpha \to \pm\pi/2$, $\beta(\pm\pi/2) = 0$. The decrease is gradual for values of α sufficiently far from $\pm\pi/2$. Near these boundaries, it is very steep. For example, the value of β is 0.25 at $\alpha = \pm 0.995\pi/2$.

The integer n_c is defined as the value of n for which $M_{c,n}$ is minimal. Therefore, $M_c = M_{c,n_c}$. The eigenmode that destabilizes the stationary distribution is a linear combination of $\exp(in_c\phi)$ and $\exp(-in_c\phi)$.

The strength of the coupling, $g_{\rm syn}$, affects only Γ_0, and not the c_n's and α_n's (Eq. 3.3). Hence, in the limit of weak coupling, M_c does not depend on $g_{\rm syn}$. Intuitively, this result stems from the fact that M_c is determined by the competition between the neuron-to-neuron fluctuations in the level of synaptic input, represented by Γ_0, and the strength of the higher components, represented by $\Gamma_0\, c_n$ (Eq. 3.4). Both factors are proportional to Γ_0, and therefore, $g_{\rm syn}$ does not affect the balance between them.

From Eq. 3.12 we see that in order to get a finite $M_{c,n}$, the condition $-\pi/2 < \alpha_n < \pi/2$ should hold. Moreover, $M_{c,n}$ is an increasing function of $|\alpha_n|$. The larger the coefficient, c_n, the smaller $M_{c,n}$ becomes.

If the transition from an asynchronous state to a state with some synchrony is supercritical, n_c determines, for $M \gtrsim M_c$, the nature of the state in which the system settles at large time for almost asynchronous initial conditions. For example, if $n_c = 1$, the system is expected to settle in a "smeared" 1-cluster state in which the phase distribution is broad but mono-modal. If $n_c = 2$, the system is expected to behave above M_c as a "smeared" 2-cluster state, characterized by bimodal phase distributions. Examples of such states are shown below.

4 Sparse networks of integrate-and-fire neurons

4.1 Estimates of M_c at weak coupling

The synaptic coupling term (Eq. 2.6) in our version of the I&F model depends only on the dynamics of the pre-synaptic neuron via the variable $s(t)$. Therefore, the effective interaction, $\Gamma(\phi)$, for this model is (Eq. 3.2)

$$\Gamma(\phi) = \frac{1}{2\pi}\int_0^{2\pi} d\psi\, Z(\psi+\phi)\, I_{\rm syn}(\psi) \tag{4.1}$$

The right-hand-side is almost a convolution integral (except for the plus sign in the function $Z\left(\psi+\phi\right)$). The phase coordinates are obtained from the time coordinate according to $\phi = \omega_0 t$ with $\omega_0 = 2\pi f_0$. The functions $Z\left(\phi\right)$ for the I&F model is (Hansel *et al.* 1995)

$$Z\left(\phi\right) = \begin{cases} 0 & 0 < \phi \leq \phi_r \\ \frac{1}{I_{\text{ext}}} e^{(\phi-\phi_r)/(\omega_0\tau_0)} & \phi_r < \phi \leq 2\pi \end{cases} \tag{4.2}$$

where $\phi_r = \omega_0 T_r$. The function $I_{\text{syn}}\left(\phi\right)$ is (Hansel *et al.* 1995)

$$I_{\text{syn}}\left(\phi\right) = \frac{g_{\text{syn}}}{\tau_2 - \tau_1}\left(\frac{e^{-\phi/(\omega_0\tau_2)}}{1-e^{-1/(f_0\tau_2)}} - \frac{e^{-\phi/(\omega_0\tau_1)}}{1-e^{-1/(f_0\tau_1)}}\right) \tag{4.3}$$

The function $V(\phi)$, $s(\phi)$, $Z(\phi)$ and $\Gamma(\phi)$ for a specific case are plotted in Fig. 1. The function $Z(\phi)$ is discontinuous at $\phi = 0$ and $\phi = \phi_r$, but the function $\Gamma(\phi)$ is continuous for all ϕ. Using the parameterization (Eq. 3.3) and the calculation reported in Appendix B, one obtains:

$$c_n = 2\left\{\left(1+n^2\,\omega_0^2\,\tau_1^2\right)\left(1+n^2\,\omega_0^2\,\tau_2^2\right)\right\}^{-1/2} \times \tag{4.4}$$

$$\left(1+n^2\,\omega_0^2\tau_0^2\right)^{-1/2}\left\{\left[1+\frac{2I_{\text{ext}}\left(I_{\text{ext}}-\theta\right)}{\theta^2}\left(1-\cos\left(n\omega_0\,T_r\right)\right)\right]\right\}^{1/2}$$

$$\alpha_n = -\pi + \frac{\pi}{2}\text{sign}\left(\text{g}_{\text{syn}}\right) + \arctan\,\text{n}\omega_0\tau_1 + \arctan\,\text{n}\omega_0\tau_2 + \arctan\,\text{n}\omega_0\tau_0 + \tag{4.5}$$

$$\arctan\frac{\sin\left(n\,\omega_0\,T_r\right)}{\left[I_{\text{ext}}/\left(I_{\text{ext}}-\theta\right)\right]-\cos\left(n\,\omega_0\,T_r\right)}$$

The first factor in Eq. 4.4 depends only on the synaptic properties, whereas the second factor reflects the intrinsic response properties of the neurons. Similarly, the first three, non-trivial, terms in Eq. 4.5 depend on the nature of the interactions and on the synaptic dynamics while the two terms in this equation depend only on the intrinsic properties of the neurons.

4.2 Inhibitory coupling, $T_r = 0$

The angle, α_n, for an inhibitory coupling and $T_r = 0$ is given by

$$\alpha_n = -\frac{3\pi}{2} + \arctan\,n\omega_0\tau_0 + \arctan\,n\omega_0\tau_1 + \arctan\,n\omega_0\tau_2 \tag{4.6}$$

The critical number, $M_{c,n}$, is finite only if $-\pi/2 < \alpha_n < \pi/2$. All the arguments of the arctan function in Eq. 4.6 are positive, therefore $\alpha_n < 0$ since the sum of the three last terms is between 0 and $3\pi/2$. To get $\alpha_n > -\pi/2$, the sum of these three terms should be larger than π, see Fig. 2A.

The coefficients, c_n, are given by

$$c_n = 2\left[\left(1+n^2\,\omega_0^2\,\tau_0^2\right)\left(1+n^2\,\omega_0^2\,\tau_1^2\right)\left(1+n^2\,\omega_0^2\,\tau_2^2\right)\right]^{-1/2} \tag{4.7}$$

Below, the implication of Eqs. 4.6 and 4.7 are listed . While reading it, it is useful to look at Fig. 2B, where α_n and c_n are plotted as a function of f_0 for $\tau_2 = 6$ ms, $\tau_1 = 5.9$ ms, and $n = 1, 2, 3$; and at the two examples in Fig. 3A, in which $M_{c,n}$ is shown as a function of f_0 for that parameter set (left) and for $\tau_1 = 1$ ms (right). The first 6 conclusions below are valid for $\tau_1 > 0$.

1. *Competition between α_n and c_n:* The angle, α_n, increases with f_0, whereas the amplitude, c_n, decreases with it (Fig. 2). Therefore, for each n, at low firing rates, α_n is smaller than $-\pi/2$, and $M_{c,n}$ is infinite. There is a critical firing rate for which $M_{c,n}$ is finite, and for slightly larger f_0, $M_{c,n}$ decreases because near $\alpha_n = -\pi/2$ the function β is very steep. For large frequencies, α_n approaches 0 and c_n continues to decrease, and therefore, $M_{c,n}$ increases. As a result, $M_{c,n}$ has a minimum as a function of f_0 at a finite value of f_0.

2. *The asynchronous state is always unstable for high enough M:* The angle, α_n, is a monotonic increasing function of n. For $\tau_1 > 0$, $\alpha_n \to 0$ for $n \to \infty$. Therefore, there is always an n_c such that $\alpha_n > -\pi/2$ for all $n > n_c$. This implies that the asynchronous state loses stability at a finite value of M, which is M_{c,n_c}.

3. *The critical mode is $n_c = 1$ at high enough values of f_0:* This is because for high enough values of f_0, $\alpha_1 > -\pi/2$ and c_1 is the minimal c_n. At very high values of f_0, $\alpha_1 \approx 0$, and from Eqs. 3.12, 4.7 and 2.9 one concludes that M_c scales like f_0^6 (or I_{ext}^6).

4. *The critical mode, n_c, increases with decreasing f_0:* This is a consequence of the facts that: I. for each specific n, α_n decreases as the firing frequency, f_0, decreases; and II. α_n increases with n. When for some n, α_n goes below $-\pi/2$, n_c is higher than that specific n.

5. *All $M_{c,n}$'s have the same minimum with respect to f_0:* For fixed τ_1/τ_0 and τ_2/τ_0, $M_{c,n}$ is a function of the variable $x = n f_0 \tau_0$. Therefore,

$$M_{c,n}\left(f_0\right) = M_{c,1}\left(n f_0\right) \tag{4.8}$$

In particular, the minima over the network parameters of all $M_{c,n}$ are the same.

6. *The critical number of synaptic connection, M_c, is non-monotone with f_0:* Here we describe the behavior of M_c as f_0 decreases. At high f_0, $n_c = 1$, and M_c decreases with decreasing f_0. At a specific value of f_0 it reaches its minimum $M_{c,1}(f_0)$ and then increases again. As f_0 continues to decrease, a value of f_0 for which $n_c = 2$ is reached, and M_c decreases again until it reaches a second minimum. Then, it increases until $n_c = 3$, decreases again and so on. More generally, M_c oscillates infinitely many times as f_0 decreases towards 0, *i.e.,* as I_{ext} decreases toward the threshold θ.

7. *Positive τ_1 is needed for destabilizing the asynchronous state:* If $\tau_1 = 0$, and in the absence of refractoriness, $\alpha_n < -\pi/2$ for all n. Therefore the asynchronous state is stable for every M. This extends, to the case of a sparse weakly coupled network, a similar result established by Van Vreeswijk in the case of all-to-all coupling (Van Vreeswijk, 1996).

8. *Effects of synaptic times:* As τ_1 increases from 0 (note that $\tau_1 \leq \tau_2$), a lower frequency is needed for $M_{c,1}$ to be finite. Since c_1 is larger at lower frequencies, the minimal value of $M_{c,1}$ as a function of f_0 is smaller at higher τ_1. For the parameters of Fig. 3A, it is 418 for $\tau_1 = 5.9\ ms$ and 2825 for $\tau_1 = 1\ ms$. The dependence of M_c on the synaptic rise and decay times at high frequency (f_0 = 102 Hz) is shown in Fig. 3B. In the left panel, $M_{c,1}$ varies with τ_1 for $\tau_2 = 6$ ms. At low τ_1, M_{c_1} is indefinite because $\alpha_1 < -\pi/2$. It increases with τ_1 for high τ_1 because c_1 decreases. Higher modes have $M_{c,n}$'s that are out of the scale of the figure. In the right panel, $M_{c,1}$ varies with τ_2 for $\tau_1 = 1$ ms. Again, it has a minimum with respect to τ_2. At small τ_2, $n_c = 2$.

We have found that the minimal number, over all the parameters of the $I\&F$ model with inhibition and $T_r = 0$, of synaptic inputs M required to destabilize the asynchronous state is obtained for $\tau_1 = \tau_2 = \tau_0$ where $M_c = 363.8$; for $\tau_0 = 10$ ms, f_0 at the minimum is 31.2 Hz. This shows that $I\&F$ neurons are hard to synchronize with inhibitory coupling in the sense that a large number of inputs are necessary to destabilize the asynchronous state of a sparse network of such neurons.

4.3 The effect of refractoriness

In the $I\&F$ model with no refractoriness, M_c is on the order of several hundreds or more. Can M_c be reduced by the inclusion of refractoriness ? To investigate this issue, we analyze the effect of T_r for fixed firing frequency, f_0. Finite T_r contributes a factor that is larger than 1 to c_n (Eq. 4.4), and a term to α_n. (Eq.4.5). This factor and term depend explicitly on $\omega_0 T_r$. They are small at low firing rates, but they can have a major effect at high firing rates.

The dependence of $M_{c,n}$, $n = 1, 2, 3$ on $I_{\rm ext}$ is presented in Fig. 4A for $T_r = 2$ ms, $\tau_2 = 6$ ms, and two values of τ_1: 5.9 ms and 1 ms. As in the case $T_r = 0$, the stability is determined by the first mode at large $I_{\rm ext}$ and by higher modes as $I_{\rm ext}$ decreases. The effect of T_r on $M_{c,n}$ is demonstrated by comparing Fig. 4A to Fig. 3A. This comparison demonstrates that the effect of the refractory period is indeed more important at high frequencies. The dependence of M_c on T_r is demonstrated in Fig. 4B for $\tau_2 = 6$ ms, $\tau_1 = 1$ ms. The level of external current, $I_{\rm ext}$, is tuned such that the frequency is fixed: $f_0 = 102$ Hz. At small T_r, $n_c = 1$. M_c decreases considerably with T_r (from 2941 at $T_r = 0$ to 141 at $T_r = 4.1$ ms), mainly because of an increase of c_1. At $T_r = 5.5$ ms, $\alpha_1 = -\pi/2$, and hence $n_c = 2$ for higher T_r.

In summary, if the mode $n = 1$, destabilizes the asynchronous state for $T_r = 0$, refractoriness decreases M_c considerably at high firing rates (as long as it is not too large), but only slightly at low firing rates.

5 Numerical simulations

5.1 Goals and methods

The analytical theory that enables us to estimate M_c, has been developed for the conditions of weak coupling, $1 \ll M \ll N$, and in the limit where $c_n \to 0$, for all n. There are several questions it cannot answer:

1. How good is the estimate of Eq. 3.12 when these conditions are not satisfied ?

2. What are the patterns of synchrony for $M > M_c$?

3. Are the qualitative predictions of the theory correct beyond the weak coupling limit ? How does M_c vary when the coupling increases ?

In order to answer these questions, we carry out numerical simulations of both the full model and the corresponding phase model.

5.1.1 Phase model

The simulations of the phase model were done as follows. The phase equations (Eq. 3.4) (without the term $2\pi f_0$ that does not affect synchronization) were integrated using a forth-order Runge-Kutta method. The time step, Δt ,was chosen such that there are at least 20 steps in a time period of the simulated model. The initial conditions for ϕ_i were chosen at random from a uniform distribution between $-\pi$ and π. The state of the network, i.e., the level and form of synchrony, was characterized by the order parameters (Kuramoto 1984)

$$Z_n = \frac{1}{T_m} \int_0^{T_m} |z_n(t)|\, dt \tag{5.1}$$

where

$$z_n = \frac{1}{N} \sum_{i=1}^{N} e^{in\phi_i} \tag{5.2}$$

and T_m is a long-enough measurement time. The first order parameter, Z_1, measures the tendency of the oscillator population to evolve in full synchrony: $Z_1 = 1$ if and only if $\phi_i(t) = \phi(t)$ for all i and t. The higher order parameters, Z_n, measure the tendency of the population to segregate into n clusters. For example, if a large population segregates into two equally-populated clusters, oscillating locked in anti-phase, $Z_2 = 1$ while $Z_1 = 0$. In the limit $N \to \infty$, $Z_n = \delta_{n,0}$ if and only if the system is in an asynchronous state. As a result, $z_n(t)$ rises from near 0 until it reaches a steady state. The order parameters,Z_n, are computed for a time period of 5000 time steps after the transients are gone. All numerical simulations are carried out with 10 realizations over which results are averaged for each set of parameters.

5.1.2 Integrate and fire network

The $I\&F$ equations (2.4, 2.5) were integrated using a second order Runge-Kutta method supplemented by a first order interpolation of the firing time at threshold as explained in (Hansel *et al.* 1998, Shelley, 1999). This algorithm is optimal for $I\&F$ neuronal networks and allows one to get reliable results for time steps, Δt, which are substantially large. The integration time step is $\Delta t = 0.25$ ms. In typical simulations, the dynamic of the network was integrated for $4 \times 10^4 - 3 \times 10^5$ time steps. Stability of the results was checked against varying the number of time steps in the simulations and their size.

The initial conditions where chosen according to:

$$V_i(0) = I_0\tau_0(1 - \exp(-b\frac{i-1}{N}\frac{(T_0 - T_r)}{\tau})) \tag{5.3}$$

$(i = 1, ..., N)$. The coefficient $0 < b < 1$ controls the degree of synchrony of the initial condition. Setting $b = 0$ yields a perfectly synchronized initial condition. On the opposite, $b = 1$ corresponds to a uniform distribution of firing times for uncoupled neurons between 0 and $T_0 - T_r$. All synaptic currents were set to 0 at $t = 0$.

To measure the degree of synchrony in the steady state of the network, we follow the method proposed and developed in (Ginzburg and Sompolinsky 1994, Golomb and Rinzel 1993, 1994, Hansel and Sompolinsky 1992) that is grounded on the analysis of the temporal fluctuations of macroscopic observables of the networks, such as the instantaneous activity of the system or the spatial average of the membrane potential. For the latter, one evaluates at a given time, t, the quantity:

$$V(t) = \frac{1}{N}\sum_{i=1}^{N} V_i(t) \tag{5.4}$$

The variance of the time fluctuations of $V(t)$ is

$$\sigma_V = \left\langle [V(t)]^2 \right\rangle_t - [\langle V(t) \rangle_t]^2 \tag{5.5}$$

where $\langle \dots \rangle_t = \int_0^{T_m} dt \ \dots$ denotes time-averaging over a large time, T_m. After normalization of σ_V to the average over the population of the single cell membrane potentials

$$\sigma_{V_i} = \left\langle [V_i(t)]^2 \right\rangle_t - [\langle V_i(t) \rangle_t]^2 \tag{5.6}$$

one defines a synchrony measure, $\chi(N)$ for the activity of a system of N neurons by:

$$\chi^2(N) = \frac{\sigma_V^2}{\frac{1}{N}\sum_{i=1}^{N} \sigma_{V_i}^2} \tag{5.7}$$

This *synchrony measure*, $\chi(N)$, is between 0 and 1. In the limit $N \to \infty$ it behaves as:

$$\chi(N) = \chi(\infty) + \frac{a}{\sqrt{N}} + O(\frac{1}{N}) \tag{5.8}$$

where a is some constant, between 0 and 1. In particular, $\chi(N) = 1$, if the system is fully synchronized (i.e., $V_i(t) = V(t)$ for all i), and $\chi(N) = O(1/\sqrt{(N)})$ if the state of the system is asynchronous. Asynchronous and synchronous states are unambiguously characterized in the thermodynamic limit (i.e., when the number of neurons is infinite). In the asynchronous state, $\chi(\infty) = 0$.

By contrast, in synchronous states, $\chi(\infty) > 0$. In homogeneous fully connected networks, an important class of partially synchronous state, ($0 < \chi(\infty) < 1$), are the "cluster states" (Golomb *et al.* 1992, Golomb and Rinzel 1994, Golomb *et al.* 1994, Hansel *et al.* 1995). In these states, the system segregates into several clusters that may fire alternately. In heterogeneous or sparse networks, the disorder can smear the clustering. For instance, in a "smeared 1-cluster state", the population voltage, $V(t)$, (Eq. 5.4) oscillates with time and has one peak as a function of time in each time period. More generally, in a "smeared n-cluster state", $V(t)$ has n peaks as a function of time in each time period.

5.1.3 Finite-size effects in sparse networks

In general, for finite N, even in the asynchronous state, $\chi(N)$ is not equal to 0. However, for finite but large N, according to Eq. 5.8, synchronous state differs from asynchronous state in the way $\chi(N)$ scales with N, i.e., by the way the finite size of the system affects the level of synchrony of the neural activity. As explained in (Hansel and Sompolinsky, 1996), these *finite size effects* can be used, in numerical simulations, to characterize the regimes of parameters in which the network states are asynchronous or synchronous. If in the thermodynamic limit, a continuous transition occurs between asynchronous and synchronous regimes when a parameter is changed (e.g., M), this transition is replaced for finite N by a crossover between the two different scalings of χ with N.

These finite size effects occur no matter what the connectivity. In networks with finite M and N, sparseness is another source of finite-size effects. The reason is that the desynchronizing effect due to the sparseness depends not only on M, but also on the relative values of M and N. For instance, in Eq. 3.4, the synchrony level in the system is determined by the competition between the term $\tilde{\Gamma}$ that may be synchronizing, and the distribution of m_i/M that tends to desynchronize the system. If M is sufficiently large, this binomial distribution of m_i/M is approximated by a Gaussian with a variance $1/M$ (Eq. 3.8). When N is finite but large enough (say, $N > 30$), and $N - M$ is also large enough, the binomial distribution of m_i/M is well-approximated by a Gaussian with a variance

$$\mathrm{Var}\left(\frac{m_i}{M}\right) = \frac{1}{M} - \frac{1}{N} \tag{5.9}$$

This suggests that the level of synchrony should depend on M and N through the effective vari-

able, M_{eff}, defined as:

$$\frac{1}{M_{\text{eff}}} = \frac{1}{M} - \frac{1}{N} \tag{5.10}$$

Relying on this heuristic argument, we expect that M_{eff} is a more appropriate parameter than M to represent simulation results.

5.2 Simulation results for weakly coupled neurons

5.2.1 Finite size effects

In Fig. 5A, we present the dependence of χ on M for $I\&F$ networks with different size, $N = 200$ to $N = 3200$. The parameter set is: $T_r = 0$, $\tau_1 = 1$ ms, $\tau_2 = 3$ ms, $I_{\text{ext}} = 2\ \text{mV/ms}$, $g_{\text{syn}} = -0.2$. The initial conditions where chosen such that $b = 0.5$ (Eq. 5.3). When N increases, the curves shift toward higher values of M. Very large values of N would be necessary in order to see that the lines converge to a limit curve. This is due to the fact that for these parameters, M_c is very large. In Fig. 5B, we present χ as a function of M_{eff} for the same values of N. It is remarkable that the lines for $N = 800, 1600, 3200$ collapse on almost the same curve. Deviations from this curve are more apparent at small values of M where one can check that χ depends on N as $1/\sqrt{N}$, which means that the network state is asynchronous there. For larger values of M_{eff}, around $M_{\text{eff}} \approx 2500$, a cross-over occurs between a regime in which $\chi = O(1/\sqrt{N})$ and a regime where χ remains finite in the large N limit. The region in which this crossover occurs is in good correspondence with our weak coupling estimate for the critical value of M above which, for this set of parameters, the asynchronous state lose stability, namely: $M_c = 2785$. For $N = 400$ and $N = 200$, $\chi(M_{\text{eff}})$ is also quite close to the effective line, although deviations are more prominent than for larger values of N.

This example shows that it is possible to estimate M_c by studying how χ depends on M_{eff} in simulation with a relatively small N (about 200-800), even though M_c is much larger than these values of N.

5.2.2 Weakly coupled inhibitory neurons

To proceed further in the comparison between the theory and the numerical simulations, we study the dependence of the synchrony level on M for three values of the external input current I_{ext}: $1.02\ \text{mV/ms}$, $1.07\ \text{mV/ms}$ and $1.12\ \text{mV/ms}$. We simulated both the phase model and the full

$I\&F$ model for inhibitory coupling with $N = 800$ neurons, $T_r = 0$, $\tau_1 = 5.9$ ms, $\tau_2 = 6$ ms and $b = 0.5$. The rise and decay times were chosen such that M_c will not be too large. Indeed, the theory for weak coupling predicts a value of M_c which is smaller by almost one order of magnitude than for $\tau_1 = 1$ ms and $\tau_2 = 3$ ms. Another prediction of the theory is that M_c (for $N \to \infty$) varies non-monotonously with $I_{\rm ext}$: $M_c = 490, 1737, 418.4$ for $I_{\rm ext} = 1.02\ {\rm mV/ms}$, $1.07\ {\rm mV/ms}$ and $1.12\ {\rm mV/ms}$ respectively. For the full I&F model, we chose $g_{\rm syn} = -0.025\ {\rm mV/ms}$. This is a weak coupling. For example, for $I_{\rm ext} = 1.12\ {\rm mV/ms}$, with this value of the coupling the firing rate of the neurons changes by less than 3%.

The results for the phase models which correspond to these parameters of the $I\&F$ network are shown in Fig. 6A. For all $I_{\rm ext}$ values, Z_1 and Z_2 are small at small M. Careful analysis shows that they scale as $1/\sqrt{N}$, indicating that at small $M_{\rm eff}$, the network is in the asynchronous state. By increasing the value of $M_{\rm eff}$, a continuous transition to a synchronous state occurs. The analytical estimates for M_c, (Eq. 5.10), for the three values of the external current are denoted by the arrows in Fig. 6. There is a very good correspondence between these values and the range of $M_{\rm eff}$ values in which Z_1 or Z_2 starts to be substantially different from 0. Note, however, that in order to estimate in a systematic way the value of M_c from the simulations, a precise finite size scaling procedure is necessary (Binder and Heermann, 1992). This is beyond the scope of this paper. The pattern of synchrony displayed by the network in the synchronous regime depends also on the value of $I_{\rm ext}$. Indeed, for $I_{\rm ext} = 1.12\ {\rm mV/ms}$, the network settles in a smeared 1-cluster state in which both Z_1 and Z_2 are $O(1)$ in the large N limit. By contrast, for $I_{\rm ext} = 1.02\ {\rm mV/ms}$ and $I_{\rm ext} = 1.07\ {\rm mV/ms}$, the pattern of synchrony is a smeared 2-cluster state characterized by $Z_2 = O(1)$ but $Z_1 = O(1/\sqrt{N})$. This is in agreement with the theory which predicts $n_c = 1$ for $I_{\rm ext} = 1.12\ {\rm mV/ms}$, and $n_c = 2$ for $I_{\rm ext} = 1.02\ {\rm mV/ms}$ and $I_{\rm ext} = 1.07\ {\rm mV/ms}$. Note that for $I_{\rm ext} = 1.07\ {\rm mV/ms}$ and $I_{\rm ext} = 1.02\ {\rm mV/ms}$ for large values of M, the system displays multistability: smeared 2-cluster states coexist with a stable smeared 1-cluster state (data not shown).

In Fig. 6B we present the results of our simulations for the full $I\&F$ networks for a synaptic strength, $g_{\rm syn} = -0.025\ {\rm mV/ms}$. Similar to the phase model, when M increases, a continuous transition occurs between the asynchronous state and a synchronous state in a range of values of $M_{\rm eff}$ which agrees with our analytical estimate for M_c. The synchrony measure χ does not discriminate between different patterns of synchrony of the full model. To characterize further these patterns, the rastergrams are plotted in Fig. 7 for $M_{\rm eff} = 600$ and the three $I_{\rm ext}$ values. We

plot also ρ, the percentage of neurons that are firing as a function of time ($1\ ms$ bins). For $I_{\rm ext} = 1.12$, simulations reveal only one group of neurons firing every cycle, i.e., the state of the system is a smeared 1-cluster, see Fig. 7A. By contrast, for $I_{\rm ext} = 1.07\ {\rm mV/ms}$ and $I_{\rm ext} = 1.02\ {\rm mV/ms}$, the network settles in a smeared 2-cluster state, see (Fig. 7B,C). These results are in agreement with what we have found for the corresponding phase models.

The theory predicts a non-monotonous variation of M_c with the external current, or equivalently with f_0, see Fig. 4. Our simulations for both the phase model and the full model are in agreement with this prediction, see Fig. 6. From this result, one expects that for fixed M, the synchrony measure, χ is a non-monotonous function of f_0. This is confirmed by our simulations as shown in Fig. 8A where we have plotted χ versus f_0 for $M_{\rm eff} = 800$ ($M = 400$ and $N = 800$). In the range of f_0 we studied, χ displayed two peaks of different amplitudes. The peak of smallest amplitude occurs for $20\ {\rm Hz} < {\rm f_0} < 30\ {\rm Hz}$. Raster plots reveal that for these values of f_0 the network settles into smeared 2-cluster states (results not shown). A second peak of larger amplitude occurs for $40\ {\rm Hz} < {\rm f_0} < 70\ {\rm Hz}$. In this range, the network settles into a smeared 1-cluster state. For $30\ {\rm Hz} < {\rm f_0} < 40\ {\rm Hz}$, the asynchronous state is stable. This is also in agreement with our analytical predictions, see Fig. 4. Interestingly, in a small range of f_0 ($37\ {\rm Hz} < {\rm f_0} < 40\ {\rm Hz}$), the network state depends on the initial conditions. Starting with initial conditions which are strongly coherent ($b = 0.95$), the network settles into a one-cluster state. By contrast, if $b = 0.1$, the asymptotic state is asynchronous. Therefore, in this range of frequencies, the system is bistable with coexistence of a stable asynchronous state and a stable smeared 1-cluster state.

The results shown in Fig. 7B suggest that for fixed firing rate, f, the synchrony measure can be a non-monotonic function of the refractory period. This prediction is checked in Fig. 8B where χ is plotted versus the refractory period for $f_0 = 102\ {\rm Hz}$ and $M_{\rm eff} = 800$ (other parameters as in Fig. 7B, $N = 800$, $M = 400$). For small refractory period, $T_r < 1$ ms, the network is in an asynchronous state. By increasing T_r, the asynchronous state becomes unstable and the synchrony increases. The network settles in a smeared 1-cluster state. However, further increasing T_r causes χ to decrease. In a small range of T_r, namely, $5.5\ {\rm ms} < {\rm T_r} < 6.5\ {\rm ms}$, the asynchronous state becomes stable again, as predicted from our analytic results, see Fig. 7B. For large values of T_r, the activity of the network synchronizes again and settles into a smeared 2-cluster state (result not shown).

We conclude that the phase model and our analytical estimation can be used to predict the

behavior of the full model with small coupling strength. Similar behaviors are observed in the simulations of the full model (Fig. 6B) for finite but not too large coupling strength.

5.3 Beyond weak coupling

Here we are interested in how M_c depends on the coupling strength in the $I\&F$ model beyond the weak coupling regime. In Fig. 9, we plot results from simulations showing the synchrony measure χ vs. M_{eff} for a fixed value of the external input, $I_{\text{ext}} = 2mV/ms$ and different coupling strength, g_{syn}. For sufficiently low values of g_{syn}, $\chi(M)$ depends weakly on g_{syn}, and M_c remains close to the weak coupling estimate although it starts to increase. For larger $-g_{\text{syn}}$ (*e.g.,* $0.5\ \text{mV/ms}$), the limit of stability of the asynchronous state becomes substantially different from its weak-coupling limit. Moreover, the system displays multistability: 1-cluster state (upper branch) coexists with asynchronous or 2-cluster state (lower branch). Therefore, increasing g_{syn} opposes synchrony, instead of helping synchrony, as one would expect at first sight. This is also clear from Fig. 10A (solid line). Here we have plotted χ versus g_{syn} for a given value of M and I_{ext}. Not only does one find that the synchrony of the system decreases when the coupling increases, but one also sees that there exists a critical coupling, $g_c(M)$, above which the network settles into an asynchronous state.

In these simulations, I_{ext} was kept fixed. Therefore, the firing rate decreased when the inhibitory coupling was increased. In order to compare networks with comparable average firing rates but different coupling strength, we have performed another set of simulations in which I_{ext} and g_{syn} increases in such a way that the average firing rate, f, in the asynchronous state was kept fixed. The results are shown on Fig. 10A (dotted line). Here also, χ is a decreasing function of $-g_{\text{syn}}$, although it varies more slowly than when the firing rate is not fixed. For a sufficiently strong coupling, $|g_{\text{syn}}| > g_c(M)$, the network settles into a state in which neurons fire in an asynchronous and (almost) periodic fashion.

By further increasing g_{syn} , one can maintain the population average firing rate constant by increasing I_{ext}. However, the neural activity becomes more and more heterogeneous across the network and the distribution of the time average firing rates of the neurons becomes broad. Simultaneously, the activity of the neurons becomes less and less periodic. This is shown in Fig. 11 for $f = 100\ Hz$, and $g_{\text{syn}} = -25\text{mV/ms}$. In this figure, we present results from the simulations of networks with different size (N=400, N=800 and N=1600), but the same M_{eff} ($M_{\text{eff}} = 800$).

Fig. 11A shows the distribution of the firing rates of the neurons. The coefficient of variations of the interspike distribution (CV) of the neurons versus their firing rates is displayed in Fig. 11B. Remarkably, the curves for the three sizes are superimposing. In Fig. 11B, the three curves are indistinguishable. This means that also in the strong coupling regime the dynamic state of the network depends only $M_{\rm eff}$.

Note that the variability in the firing pattern is stronger for the neurons with the lower rate. For fixed $g_{\rm syn}$, the lower the population average firing rate or the lower $M_{\rm eff}$, the larger the variability of the neural activity (result not shown). This is in agreement with results obtained by previous authors (van Vreeswijk and Sompolinsky, 1996, 1998; Kim *et al.* 1998).

5.4 Synchrony in sparse and heterogeneous inhibitory networks.

Until now we have investigated sparse homogeneous networks. Here we consider briefly some effects of heterogeneities. For the sake of simplicity heterogeneities are introduced as spatial fluctuations in the external input, i.e., we assume that each neuron receives an external input:

$$I_{i,\rm ext} = \bar{I}_{\rm ext} + \delta_i \tag{5.11}$$

where $\bar{I}_{\rm ext}$ is the population average of the external current and δ_i is a random number, uniformly distributed between $-\delta$ and δ. These distributions of external current can be thought of as a consequence of spatial heterogeneities in some external stimulus, or equivalently as the result of heterogeneities in the threshold of the neurons in the network.

Neltner *et al.* (Neltner *et al.* 1999), have shown that for a given level of heterogeneities, δ, the asynchronous state of a fully connected inhibitory network is destabilized if the coupling $|g_{\rm syn}|$ is larger than a critical value which is roughly proportional to δ. When the network is heterogeneous but sparse, the situation is different. This is shown in Fig. 10B where the synchrony measure, χ, is plotted as a function of $g_{\rm syn}$, for two values of δ: $\delta = 0.075{\rm mV/ms}$ and $\delta = 0.15{\rm mV/ms}$, and the same parameters as in Fig. 10A. At weak coupling, the network activity is asynchronous in both cases ($\chi = O(\sqrt{N})$). This is a consequence of the heterogeneities which prevent the neural activity to synchronize. Indeed, for $\delta = 0$ the network activity would synchronize ($M_{\rm eff} > M_c$). For $\delta = 0.075{\rm mV/ms}$, χ starts to increase above some critical value of the coupling. This signals the fact that the asynchronous state becomes unstable. the desynchronizing effect of heterogeneities. However, if the coupling increases too much, χ decreases again. This is because the

spatial fluctuations which result from the sparseness become sufficiently strong to desynchronize the network activity again. Eventually, at large coupling, the neurons fire asynchronously. For $\delta = 0.15\mathrm{mV/ms}$, the network activity remains asynchronous at any coupling value. More generally, this will be the situation if δ is too large. Therefore, one sees that in contrast to what happens in a fully connected network, there is a maximum value for δ, which depends on M, that is compatible with the emergence of synchrony.

6 Discussion

6.1 Analytical results

The analytical results reported in this article are based on two approximations. The first one is the weak coupling, in which the model can be reduced to a phase model. The conditions for which this approximation is valid have been discussed before (*e.g.,* Kuramoto 1984). Simulations of networks of identical neurons with all-to-all coupling have revealed that results based on the weak-coupling limit are also valid for intermediate coupling strengths (Hansel *et al.* 1995). A similar conclusion is obtained here. In particular, simulations of the full model with moderate coupling strength reveal values of M_c that are similar to what is obtained by simulating the reduced phase model.

Our analytical approach also relies upon a second assumption: the dynamics of a neuron is governed only by the number of synaptic inputs it receives from other neurons in the network. A more thorough analysis of this assumption (Golomb and Hansel, unpublished) reveals that it is exact in the limit $c_n \to 0$, but is only approximate for a general phase model.

Our simulations indicate that this approximation provides a good estimate of the dynamics of sparse neuronal systems. In all the cases we have examined, the differences between the theoretically-estimated values of M_c and the values of M_c obtained from simulation have been less than 20%. The good correspondence between the analytical and simulation results stems from the fact that in most cases in $I\&F$, neurons fire at not too small rate, c_1 is 0.2 or less, and c_n values with $n > 1$ are even smaller.

Our approximation means that the difference in the number of inputs between different neurons is the main source of desynchronzing disorder coming from the sparseness of the connectivity. A second source of disorder, the fact that neurons receive synaptic input from different sources

(output neurons), was found to be of minor effect in our simulations. Another type of sparse architecture which has been used in modeling neuronal systems by other authors (Whittington *et al.* 1995, Traub *et al.* 1996), consists of neurons randomly connected, but with a number of inputs which is the same for all the neurons. For such models, this second source of disorder is the only desynchronizing factor due to sparseness. Our simulations show that the network exhibits a high level of synchrony for values of M, on the order of 10 or less (data not shown, see also Wang and Buzsáki 1996 for a conductance-based model). We have also found, that the system exhibits bistability even for weak coupling, when a highly synchronized state coexists with an asynchronous state.

6.2 Patterns of synchrony for weakly coupled neurons

The nth mode of the stability matrix of the asynchronous state is unstable if: (1) $-\pi/2 < \alpha_n < \pi/2$, and (2) c_n is large enough. The first condition is identical to the instability criterion of the asynchronous state in a fully connected network. The second condition means that the modulation of the nth Fourier mode of the effective phase interaction is large enough to overcome the disorder caused by the sparse connectivity. If $M = N$, this disorder is absent, and, therefore, any modulation can destabilize the asynchronous state.

We first discuss the pattern of synchrony of inhibitory $I\&F$ networks. In that case, M_c is a non-monotonous function of the frequency, f_0 (or equivalently the external current I_{ext}), and it has many minima. At high frequency, the asynchronous state is destabilized by the first modes, whereas at lower frequencies it is destabilized by higher mode. These are consequences of the interplay between the effects of the angle, α_n, and the amplitude, c_n. For each mode, c_n decreases with frequency, and the phasic modulation of the mode decreases, but α_n is within the desynchronizing range $(-\pi/2, \pi/2)$ only for high-enough frequencies. Therefore, for each mode there is a minimal value for its critical number, $M_{c,n}$, with respect to f_0. Moreover, c_n is smaller and α_n is larger for higher n, and, therefore, these minima occur at lower frequencies for higher modes. The asynchronous state is always stable for $T_r = 0$, if the synaptic rise is instantaneous ($\tau_1 = 0$). For small τ_1, M_c is very high. However, with refractoriness, M_c can be moderate and even small, for small or zero τ_1.

Our simulations show that destabilization of the asynchronous state by the nth mode leads to an n-cluster state. This explains why cluster states are observed at low frequencies. However, for

sufficiently large M, these states coexist with smeared 1-cluster states. A consequence of this is that in numerical simulations the synchrony pattern in which the network settles depends on the initial conditions from which the simulation begins.

It should be noted that the existence of cluster states is not specific of sparse networks. Indeed, for $I\&F$ network models, cluster states can also be found in fully connected coupled networks when the synaptic time scale was fast in comparison to the firing frequency (van Vreeswijk 1996, Neltner *et al.* 1999). Cluster states have also been found in conductance-based models of inhibitory spiking neurons (Hansel et al. 1993, Wang and Buzsáki 1996). Models of thalamic networks, in which inhibitory neurons display post-inhibitory rebound, also exhibit cluster states with hyperpolarizing inhibition and fast synaptic kinetics (Golomb and Rinzel 1993, 1994; Golomb *et al.* 1994). Cluster states are, therefore, an important type of states demonstrated by various models of recurrent neuronal networks. However, their occurrence in the central nervous system has yet to be demonstrated.

6.3 Patterns of synchrony for finite coupling strength

Increasing the strength of the inhibitory synapses, (keeping the firing rate constant by increasing also the external input), has two competitive effects. On one hand, this increases the average synaptic modulation that may synchronize the system, but on the other hand, this increases the neuron-to-neuron fluctuations which tends to desynchronize the neuronal activity. For weak coupling, these two factors cancel each other and the stability of the asynchronous state is not affected by $g_{\rm syn}$; the convergence time to the synchronous state, however, is proportional to $1/|g_{\rm syn}|$. Beyond weak coupling, the synaptic inputs also distort the neuronal time course from the limit cycle of the isolated neuron, and this distortion is different for neurons that receive different numbers of inputs. Then it is not clear which of the two competitive effects is the stronger. Remarkably, in all the cases we have studied, the synchrony measure, χ, was found to *decrease* monotonously with the coupling strength, and for $g_{\rm syn}$ larger than a critical value $g_c(M)$, the network is in the asynchronous state. This suggests that the increase in the spatial fluctuations is always winning. It would be interesting to have more rigorous proof of this result.

Van Vreeswijk and Sompolinsky (1996, 1998) have studied analytically a network of sparsely connected binary neurons in the limit $1 << M << N$,$N, M \to \infty$, $g_{\rm syn}, I_{\rm ext} \propto \sqrt{M}$. They have shown that in this limit, the network settles in an asynchronous state in which the neuronal

firing is at random and is close to be a Poisson process. In this state the total input to the cells is order 1 although, excitation (from the external input) and inhibition are separately on the order of $O(\sqrt{M})$. Therefore, excitation and inhibition are "balancing" each other without any fine tuning of the parameters. More recently, Kim *et al.* (1998) have performed numerical simulations of large sparse network of $I\&F$ neurons. They have found, that under similar conditions, the network settles in a chaotic state very similar to this balanced state. Our findings that the network activity becomes asynchronous for $g_{\rm syn} > g_c(M)$ are consistent with these results. In order to further understand the dynamics of the sparse networks, it would be interesting to know how $g_c(M)$ scales with M for large M.

6.4 Behavior of more general $I\&F$ network models

The model we have studied is restricted, even in the $I\&F$ framework. We assume that the post-synaptic neuron receives a post-synaptic current immediately after the pre-synaptic neuron has fired. In cortex, there is a delay, which is about 2 ms, even between adjacent neurons (Thomson *et al.* 1993, Markram *et al.* 1997). With time delay , τ_d, the effective coupling of the phase model, Γ_d, is related to Γ by: $\Gamma_d(\phi) = \Gamma(\phi - \Delta)$ where $\Delta = 2\pi\tau_d/T_0$ (Hansel *et al.* 1995, Izhikevich 1998). Therefore, all the angles, α_n, are increased by Δ. For inhibitory coupling, a small delay reduces the frequencies at which the destabilization of the asynchronous state occurs.

The coupling in Eq. 2.4 is via "synaptic currents" in the sense that the total conductance of a cell does not depend on the synaptic input. In a version of the $I\&F$ network model which is more faithful to the biophysics, the interactions are mediated via conductance changes. The synaptic current is: $I_{syn}(t) = g_{\rm syn}(t)(V - V_{\rm rev})$, where $V_{\rm rev}$ is the synaptic reversal potential. In this case, the effective time constant τ_0 decreases with increasing the synaptic input. This is expected to have some quantitative, although not qualitative, effects on the results presented here.

The temporal summation of synaptic inputs here is assumed to be linear, and kinetic properties of synapses, such as depression or facilitation, are not considered. This is a justified assumption, provided one deals with stationary properties of the network, and the synaptic time and strength fit those of the real synapses at long time, and not in response to the initial stimulus (Markram and Tsodyks 1996).

6.5 Sparseness versus heterogeneity

Random architecture has two consequences (van Vreeswijk and Sompolinky 1998): 1) the number of inputs fluctuates from neuron to neuron; 2) different neurons receive synaptic inputs from different sources. In the approximate analytical theory we have developed in the weak coupling limit, the latter effect is neglected. That is why the instability condition of the asynchronous state (Eqs. A.18,A.19), is identical to what is found for a fully connected network of phase oscillators with random intrinsic frequencies (Sakaguchi and Kuramoto 1986, Mirollo and Strogatz 1991, Neltner *et al.* 1999), distributed according to a Gaussians distribution with an average and a variance which depends the zero-mode of the phase interaction, and therefore on the coupling strength. The good agreement of the simulations with this theory is due to the fact that for I&F neurons (and more generally for conductance-based neurons (Golomb and Hansel, unpublished)), the zero mode of the phase interaction is large in comparison to the amplitude of the first mode.

A more exact mean-field theory would require to take also into account the fact that different neurons receive synaptic inputs from different sources. This can be done in the large M, large N limit. Then, one finds that the dynamics of the sparse network is similar to the dynamics of an effective phase model with randomly distributed intrinsic frequencies and a time-correlated multiplicative noise. The properties of the noise and of the frequency distribution have to be determined self-consistently. This shows that a sparse network is not equivalent to a fully connected network with heterogeneities. However, the solution of this exact mean-field theory is difficult. We intend to study it in future work.

The difference between the effect of sparseness and of heterogeneities is also clear from our simulations at large coupling. Indeed, with a finite level of heterogeneity, a large inhibitory all-to-all network with fixed external drive becomes asynchronous with large enough $|g_{\rm syn}|$ (Wang and Buzsáki 1996, White *et al.* 1998). This is related to the decreasing in firing rate when the coupling increases. However, if the external drive is changed such that the firing rate remains fixed when the coupling strength increases, the asynchronous state becomes unstable at large enough $|g_{\rm syn}|$ (Neltner *et al.* 1999). By contrast, our simulations show that when the firing rate is kept fixed, a sparse network becomes asynchronous at large enough $|g_{\rm syn}|$.

In systems with both heterogeneities and sparseness, we have found that for not too strong coupling, χ is an increasing function of $|g_{\rm syn}|$ because the desynchronizing effect of the heterogeneities is counterbalanced by the interactions. However, for sufficiently strong coupling, the

effect of the sparseness wins. Therefore, an optimal value exists for $g_{\rm syn}$ at which χ is maximal. Note that non-monotonic variations of the synchrony level in sparse and heterogeneous network has been also found by Wang and Buzsaki (1996). However, they found it without controlling the firing rate of the neurons when the coupling is changed.

6.6 Consequences for neural modeling

In many cases, modeling large neuronal systems of the CNS in their full size would require simulating networks of ten of thousands of neurons, interacting through several millions of synapses. Simulations of such large systems are both time and memory consuming, and systematic studies of their dynamical properties using numerical simulations are hard and frequently impossible due to limitations in computer capabilities. In order to avoid these problems, systems of reduced sizes are frequently studied. However, it is not always clear how to make the size reduction of the real system. Our work suggests a simple scaling rule which can be applied to the study of patterns of synchrony in sparse network. Assume that the system one wants to study consists of N neurons connected at random, with an average number of synapses per neuron, M. Assume for simplicity that all the synapses have the same strength, G_s. Our study shows that the synchronization properties of this system can be studied by simulating a model network consisting of N_m randomly connected neurons, with average connectivity, M_m, and synaptic strength G_m, satisfying the following scaling relation:

$$G_m = \frac{M}{M_m} G_s \tag{6.1}$$

$$\frac{1}{M_m} - \frac{1}{N_m} = \frac{1}{M} - \frac{1}{N} \tag{6.2}$$

The first equation insures that the average synaptic input both in the real system and in the simulated system are the same. The second relation guarantees that the spatial fluctuations of this input are the same in both systems. As we have shown, using this scaling allows one to investigate the behavior of very large networks by simulating a network with a relatively small N_m, on the order of a few hundreds. Assuming that in the real system $1 << M << N$, N_m and M_m will not be very different. In spite of this fact, our simulation results indicate that the synchronization properties in the two systems are similar.

Synchrony in $I\&F$ inhibitory networks is very sensitive to disorder. In the context of the present work, this is expressed in the fact that M_c is large for these models. Similar conclusions

have been reached for networks of $I\&F$ with heterogeneous properties. This lack of robustness is a consequence of the purely passive integration of the synaptic and external inputs. However, even within the $I\&F$ framework, refractoriness can improve substantially the robustness of the synchrony by decreasing M_c, as we have shown. Synchrony in conductance-based neurons which take into account more biophysics of neurons, seems to be more robust (Wang and Buzsáki 1996, Neltner 1999, Golomb and Hansel, unpublished). The patterns of synchrony for $M > M_c$ can also depend on the active properties and their kinetics. For example, for the conductance-based model of Wang and Buzsáki (1996), the network settles into a smeared one-cluster state except for very low frequencies. With slower kinetics of the intrinsic currents, the second mode destabilizes the asynchronous state for all the frequency range (Golomb and Hansel, preliminary results). In that case, the network may settle into a 2-cluster state. Therefore, the role of intrinsic properties of the neurons is as important as the role of the synaptic properties in determining when synchrony can emerge in the neural activity of large networks. Nevertheless, our study points out qualitative trends regarding the role of active properties in the emergence of synchrony which have the effect of reducing M_c. However, one cannot draw general *quantitative* conclusions regarding the minimal number of synaptic inputs required for synchrony to emerge since this number can vary by one order of magnitude or more, depending on the model one considers. This raises an important issue for neural modeling: under which conditions can a conductance-based dynamics be reduced to an $I\&F$ dynamics without loosing synchronization properties?

6.7 Consequences for the mechanisms of neural synchrony

Finally, we would like to discuss some consequences of our results for the possible mechanisms underlying neural synchrony in the CNS. It has been recently proposed that inhibitory neurons could play a central role in the emergence of synchrony in large networks in the CNS. According to these ideas, synchronous rhythmic oscillations would emerge in the subnetwork of inhibitory interneurons and would subsequently entrain other populations of neurons in the system. This mechanism is supported by theoretical considerations. Indeed, it has been realized that it is easier to achieve coherent activity in fully connected networks of identical neurons if the interactions are inhibitory than if the interactions are excitatory. Note that for that to be true, no specific active properties of the neurons are required. Recent studies have pointed out that because of the heterogeneities, synchrony in inhibitory networks can be a problem, especially at moderate or high

firing rates. Nevertheless, as it has been demonstrated in (Neltner et al. 1999), the desynchronizing effect of heterogeneities of fully connected networks can be overcome provided the external input and the synaptic interactions are sufficiently strong. In the present work, we have seen that if the network is sparsely connected, increasing the interaction is desynchronizing. Hence, the capability of compensating for the heterogeneities in the strong coupling regime is opposed by the amplification in this regime of the spatial fluctuations due to the sparseness. To characterize this limitation in a more quantitative manner, more specific information is needed about the intrinsic active properties of the interneurons and about the degree of connectivity of networks of interneurons in the CNS. However, the present work shows a fundamental limitation for the mechanism of synchrony relying solely on inhibition. An important issue is, therefore, whether more robust synchrony in the CNS can be achieved through recurrent inhibition between excitatory and inhibitory populations. Work is in progress in this direction.

Acknowledgments

We are thankful to C. van Vreeswijk, G. Mato, H. Sompolinsky, L. Neltner and G.B. Ermentrout for most helpful discussions. We thank C. van Vreeswijk for careful reading of the manuscript. D.H. acknowledges hospitality of the Center for Neural Computation and the Racah Institute of Physics of the Hebrew University. This research was partially supported by the PICS 236 (PIR Cognisciences and M.A.E): " Dynamique neuronale et codage de l'information: Aspects physiques et biologiques" to D.H., and by a grant from the Israel Science Foundation to D.G.

7 Appendix A: Analytical estimate of M_c in the weak coupling limit

We assume that the state of the network at time t can be completely characterized by the density function $\rho(\phi, t, m)\, d\phi$ which is the fraction of neurons with exactly m inputs whose phase lies between ϕ and $\phi + d\phi$ at time t. Under this assumption, one can write the continuity equation for $\rho(\phi, t, m)$ which reads:

$$\frac{\partial \rho(\phi, t, m)}{\partial t} = \tag{A.1}$$

$$-\frac{\partial}{\partial \phi}\left\{\rho(\phi, t, m)\left[\frac{2\pi}{T_0} + \frac{m\Gamma_0}{M} + \frac{m}{M}\int_0^N dm'\, P_0(m', M)\int_{-\pi}^{\pi} d\phi'\, \rho(\phi', t, m')\,\tilde{\Gamma}(\phi - \phi')\right]\right\}$$

The right hand side term in Eq. A.1 means that a neuron receives phasic contribution from m other neurons, and the state of the "ancestor" neurons is determined by the number of input m' they receive themselves. Because $M >> 1$, the contribution from the "tails" of the Gaussian distribution (3.8) to the integral $\int_0^N dm'$ is negligible, and, therefore, this integral is well-approximated by $\int_{-\infty}^{\infty} dm'$. The following transformations

$$\delta m = m - M, \qquad \hat{t} = |\Gamma_0|\, t, \qquad \hat{\phi} = \phi - \left(\frac{2\pi}{T_0} + \Gamma_0\right) t \tag{A.2}$$

lead to

$$\frac{\partial \rho\left(\hat{\phi}, \hat{t}, \delta m\right)}{\partial \hat{t}} = -s_0\, \frac{\delta m}{M}\, \frac{\partial \rho\left(\hat{\phi}, \hat{t}, \delta m\right)}{\partial \hat{\phi}} \tag{A.3}$$

$$-\frac{1}{|\Gamma_0|}\left(1 + \frac{\delta m}{M}\right)\frac{\partial}{\partial \hat{\phi}}\left[\rho\left(\hat{\phi}, \hat{t}, \delta m\right)\int_{-\infty}^{\infty} d(\delta m)\; P(\delta m, M)\int_{-\pi}^{\pi} d\hat{\phi}'\, \rho\left(\hat{\phi}', \hat{t}, \delta m\right)\tilde{\Gamma}\left(\hat{\phi} - \hat{\phi}'\right)\right]$$

where $s_0 = \mathrm{sign}(\Gamma_0)$ and $\mathrm{sign(x)} = 1$ if $x > 0$ and -1 if $x < 0$. From now on, we will omit the symbol, $\hat{}$, in Eq. A.3 and refer to the values t, ϕ, as the new values defined in Eq. A.2. A trivial solution of Eq. A.3 is:

$$\rho(\phi, t, \delta m) = \frac{1}{2\pi} \tag{A.4}$$

It corresponds to the asynchronous state of the network. For analyzing its stability, we follow the approach of Strogatz and Mirollo (1991). We investigate the evolution of small deviations around this solution:

$$\rho(\phi, t, \delta m) = \frac{1}{2\pi} + \eta(\phi, t, \delta m) \tag{A.5}$$

Using Eq. 3.3 and expanding $\eta(\phi, t, \delta m)$ in Fourier series

$$\eta(\phi, t, \delta m) = \sum_{n=1}^{\infty} \left[B_n(t, \delta m)\, e^{in\phi} + c.c. \right] \tag{A.6}$$

one finds:

$$\frac{\partial B_n(t, \delta m)}{\partial t} = \tag{A.7}$$

$$-in\, s_0\, \frac{\delta m}{M}\, B_n(t, \delta m) + \frac{1}{2} \left(1 + \frac{\delta m}{M}\right) n\, c_n\, e^{i\alpha_n} \int_{-\infty}^{\infty} d(\delta m')\; B_n(t, \delta m')\, P(\delta m', M)$$

We seek for each n a solution for Eq. A.7 of the form

$$B_n(t, \delta m) = b_n(\delta m)\, e^{\lambda_n t} \tag{A.8}$$

where the eigenvalue, λ_n, does not depend on δm.

Solving Eqs.A.7,A.8 for $b_n(\delta m)$, we find

$$b_n(\delta m) = \frac{\left(1 + \frac{\delta m}{M}\right) A_n}{\lambda_n + in\, s_0\, \frac{\delta m}{M}} \tag{A.9}$$

where A_n is determined by the self-consistent equation:

$$A_n = \frac{n}{2}\, c_n\, e^{i\alpha_n} \int_{-\infty}^{\infty} d(\delta m)\, P(\delta m, M)\, b_n(\delta m) \tag{A.10}$$

The complex number λ_n can be written as $\lambda_n = \mu_n - in\Omega_n$, where μ_n and Ω_n are real. Using this notation, the complex equations A.9,A.10 are expressed as:

$$\frac{2\cos\alpha_n}{n\, c_n} = \int_{-\infty}^{\infty} d(\delta m)\, P(\delta m, M)\, \frac{\mu_n \left(1 + \frac{\delta m}{M}\right)}{\mu_n^2 + n^2 \left(s_0\, \frac{\delta m}{M} - \Omega_n\right)^2} \tag{A.11}$$

$$\frac{2\sin\alpha_n}{n\, c_n} = \int_{-\infty}^{\infty} d(\delta m)\, P(\delta m, M)\, \frac{n \left(s_0\, \frac{\delta m}{M} - \Omega_n\right) \left(1 + \frac{\delta m}{M}\right)}{\mu_n^2 + n^2 \left(s_0\, \frac{\delta m}{M} - \Omega_n\right)^2} \tag{A.12}$$

The term $\delta M/M$ is of the order $1/\sqrt{M}$. Since $M >> 1$ (Eq. 3.6), we neglect this term in Eqs. A.11 and A.12 in comparison to 1, but not in comparison to $|\Omega_n|$ that may be small. We want to find the critical value, $M_{c,n}$, above which λ_n has a positive real part ($\mu_n > 0$). Hence, we look for a solution, $M_{c,n}$, for equations A.11, A.12 in the limit $\mu_n \to 0^+$. The right-hand-side of Eq. A.11 is always positive for $\mu_n \geq 0$, and, therefore, this equation has a solution only if

$$-\pi/2 < \alpha_n < \pi/2 \tag{A.13}$$

Using the fact that $\lim_{\mu_n \to 0^+} \int_\infty^\infty d\nu \mu_n / \left(\mu_n^2 + \nu^2\right) = \pi \delta\left(0\right)$, defining $y_n = \sqrt{M_{c,n}}\, \Omega_n$, and using the identity

$$P\left(m, M\right) = \frac{1}{\sqrt{M}} P\left(\frac{m}{\sqrt{M}}\,,\, 1\right) \tag{A.14}$$

Eq. A.11 yields (after some straightforward algebra):

$$\frac{2\cos\alpha_n}{c_n} = \pi\, P\left(y_n, 1\right) \sqrt{M_{c,n}} \tag{A.15}$$

Similarly, one takes the limit $\mu_n \to 0^+$ in Eq. A.12 which gives:

$$\frac{\sin\alpha_n}{c_n} = \sqrt{M_{c,n}} J\left(y_n, 1\right) \tag{A.16}$$

where following Sakaguchi and Kuramoto (1986), we have defined

$$J\left(\Omega, M\right) = \int_0^\infty \frac{dx}{2x} \left[P\left(\Omega + x, M\right) - P\left(\Omega - x, M\right)\right] \tag{A.17}$$

Therefore, $M_{c,n}$ and Ω_n are computed from:

$$J\left(y, 1\right) = \frac{\pi}{2} P\left(y, 1\right) \tan\alpha_n \tag{A.18}$$

$$M_{c,n} = \left(\frac{2\cos\alpha_n}{\pi c_n P\left(y, 1\right)}\right)^2 \tag{A.19}$$

These equations are similar to those obtained by Sakaguchi and Kuramoto (1986) for the emergence of a synchronized state in a heterogeneous phase model with coupling via the first mode only : $\Gamma\left(\phi\right) = \sin\left(\phi + \alpha\right)$. The value of y obtained from solving Eq. A.18 is a function of α_n only. In Fig. 12A, we plot the graphs of the functions $J\left(y, 1\right)$ and $P\left(y, 1\right) \tan\alpha$ for $\alpha = -\pi/4$. It is clear that y increases with $|\alpha|$ for $|\alpha| < \pi/2$, and therefore $P\left(y, 1\right)$ decreases with $|\alpha|$ in this range. We define the universal function, $\beta\left(\alpha\right)$, to be

$$\beta\left(\alpha\right) = \frac{\sqrt{2\pi} P\left(y, 1\right)}{\cos\alpha} \tag{A.20}$$

(Fig. 12B) where y is the solution of Eq. A.18. Eq. A.19 and A.13 become:

$$M_{c,n} = \frac{8}{\pi c_n^2 \beta^2\left(\alpha_n\right)} \;\; ; \qquad -\pi/2 < \alpha_n < \pi/2 \tag{A.21}$$

Eq. A.21 gives the number of input, $M_{c,n}$, above which the nth Fourier mode destabilizes the asynchronous state. In order to find the number M_c above which this state becomes unstable, we look for the minimal $M_{c,n}$

$$M_c = \min_n M_{c,n} \tag{A.22}$$

where the minimum is over all the positive integer, n, values for which $-\pi/2 < \alpha_n < \pi/2$.

Below M_c, the asynchronous state can be stable or marginally stable. In the case of the Kuramoto model (Kuramoto 1984), the asynchronous state is linearly marginally stable when it is not unstable, in the sense that the stability matrix has a zero eigenvalue. Still, fluctuations of the asynchronous state decay with time. (Strogatz and Mirollo 1991, Strogatz *et al.* 1992). This is probably also the situation here. Our numerical results show that below M_c, the system dynamics converge to the asynchronous state when the initial conditions are chosen from a uniform distribution.

Note that the instability criterion we have established is formally similar to the equations which determine the stability boundary of the asynchronous state in a *fully connected* network of neurons with *heterogeneous* intrinsic properties (Neltner *et al.* 1999).

8 Appendix B: The Fourier Transform of $\Gamma(\phi)$

The Fourier transform of a periodic function $h(\phi)$, in the complex exponential representation, is

$$h(\phi) = \sum_{n=-\infty}^{\infty} h_n \, e^{-in\phi} \tag{B.1}$$

The complex number, h_n, is represented as $h_n = |h_n| \exp[i \arg(h_n)]$, where $|h_n|$ is non-negative and $-\pi/ < \arg(h_n) \leq \pi$. For a real number x, $\arg(x) = 0$ if $x > 0$ and $\arg(x) = \pi$ if $x < 0$. It is straightforward to calculate the Fourier coefficients of the functions $Z(\phi)$ (Eq. 4.2) and $I_{\rm syn}(\phi)$ (Eq. 4.3). One finds:

$$|Z_n| = \frac{\theta}{I_{\rm ext}(I_{\rm ext}-\theta)} \frac{1}{T_0(1+n^2\omega_0^2\tau_0^2)^{1/2}} \left\{1 + \frac{2I_{\rm ext}(I_{\rm ext}-\theta)}{\theta^2}[1-\cos(n\omega_0 T_r)]\right\}^{1/2} \tag{B.2}$$

$$\arg(Z_n) = -\arctan n\omega_0\tau_0 - \arctan \frac{\sin(n\omega_0 T_r)}{[I_{\rm ext}/(I_{\rm ext}-\theta)] - \cos(n\omega_0 T_r)} \tag{B.3}$$

$$|I_{\rm syn,n}| = \frac{|g_{\rm syn}|\ \tau_0}{T_0^2\left[(1+n^2\omega_0^2\tau_1^2)(1+n^2\omega_0^2\tau_2^2)\right]^{1/2}} \tag{B.4}$$

$$\arg(I_{\rm syn,n}) = \arg(g_{\rm syn}) + \arctan(n\omega_0\tau_1) + \arctan(n\omega_0\tau_2) \tag{B.5}$$

where the function $\mathtt{arctan}$ takes values in the interval $[-\pi/2, \pi/2]$. The convolution theorem implies that the Fourier components of $\Gamma(\phi)$ (in the complex exponential representation) are given by

$$\Gamma_n = Z_n I^*_{\mathrm{syn,n}} \tag{B.6}$$

where the asterisk means complex conjugate. Transferring this representation to the $\mathtt{sin}$ representation (Eq. 3.3), this formula becomes

$$c_n = \frac{2\,|Z_n|\;|I_{\mathrm{syn,n}}|}{|Z_0|\;|I_{\mathrm{syn},0}|} \tag{B.7}$$

$$\alpha_n = -\frac{\pi}{2} - \arg(Z_n) + \arg(I_{\mathrm{syn,n}}) \tag{B.8}$$

Eqs. B.6, B.7, B.8 are valid for every model in which the synaptic coupling is expressed in terms of currents (and not in terms of conductances). Substituting Eqs. B.2–B.5 into Eqs. B.7 and B.8 yields Eqs. 4.4, 4.5

References

Abbott L.F. and van Vreeswijk C. (1993). Asynchronous states in networks of pulse-coupled oscillators. *Phys. Rev.* **E48**, 1483-1490.

Barkai, E., Kanter, I., and Sompolinsky, H. (1990). Properties of sparsely connected excitatory neural networks. *Phys. Rev. A* **41**, 590-597.

Binder, K. and Heermann, D. W. (1992). *Monte Carlo Simulation in Statistical Physics*, Springer Verlag, Berlin.

Bressloff, P.C., and Coombes, S. (1998a) Desynchronization, mode locking, and bursting in strongly coupled integrate-and-fire oscillators. *Phys. Rev. Lett.* **81**, 2168-2171.

Bressloff, P.C., and Coombes, S. (1998b) Spike train dynamics underlying pattern formation in integrate-and-fire oscillator network. *Phys. Rev. Lett.* **81**, 2384-2387.

Brunel, N., and Hakim, V. (1999) Fast global oscillations in networks of integrate-and-fire neurons with low firing rates. Preprint.

Buzsáki, G., and Chrobak, J.J. (1995). Temporal structure in spatially organized neuronal ensembles: a role for interneuron networks. *Curr. Opin. Neurobiol.* **5**, 504-510.

Buzsáki, G., Leung, L., and Vanderwolf, C.H. (1983). Cellular bases of hippocampal EEG in the behaving rat. *Brain Res. Rev.* **6**, 139-171.

Chow, C.C. (1998). Phase-locking in weakly heterogeneous neuronal networks. *Physica D* **118**, 343-370.

Chow, C.C., White, J.A., Ritt, J., and Kopell, N. (1998). Frequency control in synchronized networks of inhibitory neurons. *J. Comput. Neurosci.* **5**, 407-420.

Ermentrout, G.B., and Kopell, N. (1984). Frequency plateaus in a chain of weakly coupled oscillators. *SIAM J. Math. Anal.* **15**, 215-237.

Gerstner, W. (1999). Population dynamics of spiking neurons: fast transients, asynchronous states, and locking. *Neural Comput.*, accepted for publication.

Gerstner, W., van Hemmen, J.L., and Cowan, J. (1996). "What matters in neuronal locking", *Neural Comput.* **8**, 1653-1676.

Ginzburg, I., and Sompolinsky, H. (1994). Theory of correlations in stochastic neuronal networks. *Phys. Rev. E* **50**, 3171-3191.

Golomb, D., Hansel, D., Shraiman, B. and Sompolinsky, H. (1992). Clustering in globally coupled phase oscillators. *Phys. Rev. A* **45**, 3516-3530.

Golomb, D. and Rinzel, J. (1993). Dynamics of globally coupled inhibitory neurons with heterogeneity. *Phys. Rev. E* **E 48**, 4810-4814.

Golomb, D. and Rinzel, J. (1994). Clustering in globally coupled inhibitory neurons, *Physica* **D 71**, 259-282.

Golomb D., Wang X.J. and Rinzel J. (1994). Synchronization properties of spindle oscillations in a thalamic reticular nucleus model, *J. Neurophysiol.* **72**, 1109-1126.

Gray C.M. (1994). Synchronous oscillations in neuronal systems: mechanisms and functions. *J. Comp. Neurosci.* **1**, 11-38.

Hansel D., Mato G. and Meunier C. (1993a). Phase dynamics for weakly coupled Hodgkin-Huxley neurons. *Europhys. Lett.* **23**, 367-372.

Hansel D., Mato G. and Meunier C. (1993b). Clustering and slow switching in globally coupled phase oscillators. *Phys. Rev* **E48**, 3470-3477.

Hansel, D., Mato, G. and Meunier, C. (1993c). Phase reduction and neural modeling. in *Functional Analysis of the brain based on multiple-site recordings*, *Concepts in Neuroscience* **4**, 192-210.

Hansel D., Mato G. and Meunier C. (1995). Synchrony in excitatory neural networks. *Neural Comp.* **7**, 307-337.

Hansel D., Mato G., Meunier C., and Neltner, L. (1998). On numerical simulations of integrate-and-fire neural networks. *Neural Comp.* **10**, 467-485.

Hansel, D., and Sompolinsky, H. (1992). Synchrony and computation in a chaotic neural network. *Phys. Rev. Lett.* **68**, 718-721.

Hansel, D., and Sompolinsky, H. (1996). Chaos and synchrony in a model of a hypercolumn in visual cortex. *J. Comp. Neurosci.* **3**, 7-34.

Izhikevich, E.M. (1998). Phase models with explicit time delays. *Phys. Rev. E* **58**, 905-908.

Kim, J., van Vreeswijk C. and Sompolinsky H. (1998). Stochastic activity in balanced integrate-and-fire neural networks. Unpublished.

Kopell, N. (1988). Toward a theory of modeling central pattern generators. In *Neural control of rhythmic movements in vertebrates*, A. Cohen Editor, 369-413, J. Wiley.

Kuramoto Y., (1984). *Chemical Oscillations, Waves and Turbulence* (Springer, New York).

Kuramoto Y., (1991). Collective synchronization of pulse-coupled oscillators and excitable units. *Physica D* **50**, 15-30.

Lytton, W.W., and Sejnowski, T.J. (1991). Simulations of cortical pyramidal neurons synchronized by inhibitory interneurons. *J. Neurophysiol.* **66**, 1059-1079.

Markram, H., Lubke, J., Frotscher, M., Roth, A., and Sakmann, B. (1997). Physiology and anatomy of synaptic connections between thick tufted pyramidal neurones in the developing rat neocortex. *J. Physiol. (Lond)* **500**, 409-440.

Markram, H., Tsodyks, M. (1996). Redistribution of synaptic efficacy between neocortical pyramidal neurons. *Nature* **382**, 807-810.

Mirollo R.E. and Strogatz S.H. (1990). Synchronization of pulse-coupled biological oscillators, *SIAM J. Appl. Math.* **6**, 1645-1657.

Neltner, L., Hansel, D., Mato, G., and Meunier, C. (1999). Synchrony in heterogeneous networks of spiking neurons. To be submitted for publication.

Sakaguchi, H., and Kuramoto, Y. (1986). A solvable active rotator model showing phase transitions via mutual entrainment. *Prog. Theor. Phys.* **56**, 576-581.

Shelley, M. (1999). Efficient and accurate integration schemes for systems of integrate-and-fire neurons. Preprint.

Strogatz, S.H., and Mirollo, R.E. (1991). Stability of incoherence in a population of coupled oscillators. *J. Stat. Phys.* **63**, 613-635.

Strogatz, S.H., Mirollo, R.E., and Matthews, P.C. (1992). Coupled nonlinear oscillations below the synchronization threshold: relaxation be generalized Landau damping. *Phys. Rev. Lett.* **68**, 2370-2373.

Thomson, A.M., Deuchars, J., and West, D.C. (1993). Large, deep later pyramid-pyramid single axon EPSPs in slices of rat motor cortex display paired pulse and frequency-dependent depression,

mediated presynaptically and self-facilitation, mediated postsynaptically. *J. Neurophysiol.* **70**, 2354-2369.

Tiesinga, P.H.E, and Jose, J.V. (1999). Robust gamma oscillations in networks of inhibitory hippocampal interneurons. Preprint, http://xxx.lanl.gov/abs/cond-mat/9904271.

Traub, R.D., Whittington, M.A., Colling, S.B., Buzsàki, G., and Jefferys, J.G.R. (1996). Analysis of gamma rhythms in the rat hippocampus *in vitro* and *in vivo*, *J. Physiol.* **493**, 471-484.

Treves A. (1993). Mean field analysis of neuronal spike dynamics, *Network* **4**, 259-284.

Tsodyks M., Mitkov I. and Sompolinsky H. (1993). Patterns of synchrony in integrate and fire network, *Phys. Rev. Lett.*, **71**, 1280-1283.

Tsodyks M. and Sejnowski T. (1995). Rapid state switching in balanced cortical network models, *Network* **6**, 111-124. Tuckwell H.C. (1988). Introduction to theoretical neurobiology, Cambrdige

University Press, New York.

van Vreeswijk, C. (1996). Partial synchronization in populations of pulse-coupled oscillators, *Phys. Rev. E* **54**, 5522-5537

van Vreeswijk, C., Abbott, L.F., and Ermentrout, G.B. (1994). When inhibition not excitation synchronizes neural firing. *J. Comput. Neurosci.* **1**, 313-321.

van Vreeswijk C. and Sompolinky H. (1996). Chaos in neuronal networks with balanced excitatory and inhibitory activity, *Science* **274**, 1724-172.

van Vreeswijk C. and Sompolinsky H. (1998). Chaotic balanced state in a model of cortical circuits, *Neural Comp.* **10**, 1321-1372.

Wang, X.-J., and Buzsáki, G. (1996). Gamma oscillation by synaptic inhibition in a hippocampal interneuronal network model. *J. Neurosci.* **16**, 6402-6413.

Wang, X.-J., Golomb, D. and Rinzel, J. (1995). Emergent spindle oscillations and intermittent burst firing in a thalamic model: specific neuronal mechanisms. *Proc. Natl. Acad. Sci. (USA)* **2**, 5577-5581.

White, J.A., Chow, C.C., Ritt, J., Soto-Treviño, C., and Kopell, N. (1998). Synchronous oscillations in heterogeneous, mutually inhibited neurons. *J. Comput. Neurosci.* **5**, 5-16.

Whittington, M.A., Traub, R.D, and Jefferys, J.G.R. (1995). Synchronized oscillations in interneuron networks driven by metabotropic glutamate receptor activation. *Nature* **373**, 612-615.

Figure Captions

Figure 1. The functions $V(\phi)$ (normalized to θ), $s(\phi)$, $Z(\phi)$ and $\Gamma(\phi)$ (normalized to $|g_{\rm syn}|$) for the $I\&F$ model with no refractory period ($T_r = 0$) and inhibitory coupling ($g_{\rm syn} < 0$). Parameters: $\tau_1 = 5.9$ ms, $\tau_2 = 6$ ms, $I_{\rm ext} = 1.12$ mV/ms, $f_0 = 44.8$ Hz.

Figure 2. A. Schematic demonstration of the condition needed to achieve $\alpha_n > -\pi/2$ for the I&F model with inhibitory coupling and $T_r = 0$. The sum of the three angles, denoted by the three levels of shading, should be larger than π for achieving this condition. The angle, $\arctan(n\,\omega_0\,\tau_0)$, stems from the contribution of the response function, Z, of the I&F neuron to the Γ function (Eq. 4.2), whereas the two angles, $\arctan(n\,\omega_0\,\tau_1)$ and $\arctan(n\,\omega_0\,\tau_2)$, stem from the contribution of the two exponents in the synaptic coupling function, $I_{\rm syn}$ (Eq. 4.3). B. The dependence of α_n (I) and c_n (II) on f_0 for $T_r = 0$, $\tau_1 = 5.9$ ms, $\tau_2 = 6$ ms; $n = 1, 2, 3$. The angle, α_n, increases with $I_{\rm ext}$, whereas the coefficient, c_n, decreases with it. For a given $I_{\rm ext}$, α_n increases with n while c_n decreases with it.

Figure 3. The first three critical numbers of inputs $M_{c,n}$ for an $I\&F$ model with inhibitory coupling and $T_r = 0$. The graphs of $M_{c,n}$ are denoted by the solid, the dotted and the dashed lines for $n = 1, 2, 3$, respectively. A. $M_{c,n}$ versus f_0 for $\tau_2 = 6$ ms and $\tau_1 = 5.9$ ms (left) or $\tau_1 = 1$ ms (right). Both figures demonstrate the non-monotonicity of M_c, the minimal $M_{c,n}$, as a function of $I_{\rm ext}$. B. $M_{c,n}$ versus τ_1 for $\tau_2 = 6$ ms (left) and versus τ_2 for $\tau_1 = 1$ ms (right). In both cases, $I_{\rm ext} = 1.6$ mV/ms ($f_0 = 102$ Hz). In the left panel, $M_{c,2}$ and $M_{c,3}$ are too large to be plotted; in the right panel, $M_{c,3}$ is not plotted for the same reason. The scale for τ_2 starts from 1 ms because $\tau_2 \geq \tau_1$ by definition.

Figure 4. Effects of refractory period, T_r. The first three critical numbers of inputs $M_{c,n}$ are plotted for an $I\&F$ model with inhibitory coupling and $\tau_2 = 6$ ms. The graphs of $M_{c,n}$ are denoted by the solid, the dotted and the dashed lines for $n = 1, 2, 3$, respectively. A. $M_{c,n}$ versus f_0 for $T_r = 2$ ms and $\tau_1 = 5.9$ ms (left) or $\tau_1 = 1$ ms (right). B. $M_{c,n}$ versus T_r for $\tau_1 = 1$ ms , ($f_0 = 102$ Hz).

Figure 5. Simulations of the $I\&F$ model with $T_r = 0$, $\tau_1 = 1$ ms, $\tau_2 = 3$ ms, $I_{\rm ext} = 2$ mV/ms ($f_0 = 144.3$ Hz), $g_{\rm syn} = -0.2$, $b = 0.5$. Simulations are carried out with $N = 200$, averaged over

100 realizations of the network connectivity and random initial conditions (dots), $N = 400$, 50 realizations (crosses), $N = 800$, 25 realizations (dashed line), $N = 1600$, 20 realizations (dotted line) and $N = 3200$, 10 realizations (solid line). The integration time step $\Delta t = 0.25$ ms; The runs were performed over 4×10^4 time steps. The synchrony measure was computed after discarding a transient of 2×10^4 time steps. A. The synchrony measure χ versus M. B. The synchrony measure χ versus M_{eff} (Eq. 5.10). The lines for $N = 800, 1600, 3200$ almost coincide with each other, and the deviations of the line with $N = 400$ and $N = 200$ is small. The analytical estimate for M_c is denoted by the arrow. Note that for $M_{\text{eff}} \lesssim 2500$, χ decreases with N: $\chi \propto 1/\sqrt{N}$.

Figure 6. Simulations of inhibitory $I\&F$ networks. Parameters: $T_r = 0$, $\tau_1 = 5.9$ ms, $\tau_2 = 6$ ms, $N = 800$. Three values of I_{ext} are used: $1.02\ \text{mV/ms}$ ($f_0 = 25.4$ Hz); $1.07\ \text{mV/ms}$ ($f_0 = 36.7$ Hz); $1.12\ \text{mV/ms}$ ($f_0 = 44.8$ Hz). A. The order parameters Z_1 and Z_2 in the reduced phase model vs. M_{eff}. Integration time step is 0.1. The results are averaged over 5×10^3 time steps (after a discarded transient of 5×10^3 time steps) and 10 realizations of the network architecture and initial conditions (homogeneous distribution between 0 and 2π). The error bars represent the standard deviation of Z. The arrows denote the analytical estimates for M_c. B. The synchrony measure χ in the full $I\&F$ model with $g_{\text{syn}} = -0.025\ \text{mV/ms}$. Time averaging over 8×10^4 time steps; discarded transient 8×10^4; $\Delta t = 0.025$ ms; 25 realizations; the initial conditions are chosen at random with $b = 0.5$. The error bars represent the standard deviation of χ.

Figure 7. Simulations of networks of inhibitory $I\&F$ neurons. Parameters are the same as in Fig. 6, and $M = 600$. Rastergrams of 400 neurons out of $N = 800$ are shown in the upper panels. Initial conditions are such that $b = 0$. A bar denoting the time period, T_0, is shown above each rastergram. In each lower panel ρ, the number of firing neurons within a time bin of 1 ms, is displayed as a function of time. For $I_{\text{ext}} = 1.12\ \text{mV/ms}$ (A) the system is in a smeared 1-cluster state, whereas for $I_{\text{ext}} = 1.07\ \text{mV/ms}$ (B) and $I_{\text{ext}} = 1.02\ \text{mV/ms}$ (C) it is in a 2-cluster state.

Figure 8. Simulation of the full $I\&F$ network with $N = 800$, integration time step: $\Delta t = 0.25$ ms. (A) The synchrony measure χ vs. the frequency f_0 for $T_r = 0$, $\tau_1 = 5.9$ ms, $\tau_2 = 6$ ms, $g_{\text{syn}} = -0.025\ \text{mV/ms}$, $M = 450$ (corresponding to $M = 1028.6$ in the limit $N \to \infty$). Results were averaged over 40 realizations of the network architecture and initial conditions. $b = 0.95$ and $b = 0.1$; 2.4×10^5 time steps (discarded transient of 1.8×10^5 time steps); (B) The synchrony measure χ vs. the refractory period T_r. The applied current was changed such that $f_0 = 102\ Hz$.

Other parameters: $g_{\rm syn} = -0.1$ mV/ms, $M = 400$ (corresponding to $M = 800$ in the limit $N \to \infty$), $\tau_1 = 1$ ms, $\tau_2 = 6$ ms. All the runs had 3×10^5 time steps. Time averages were computed after discarding a transient of 1.5×10^5 time steps. The results were averaged over 50 realizations. ($b = 0.95$ and $b = 0.1$).

Figure 9. Beyond weak coupling: simulations of the full inhibitory $I\&F$ network. The synchrony measure χ is plotted vs. $M_{\rm eff}$ for different synaptic strength. Parameters are: $T_r = 2$ ms, $\tau_1 = 1$ ms, $\tau_2 = 3$ ms, $I_{\rm ext} = 2$ mV/ms, ($f = 112\ Hz$) $N = 800$. Simulations with 4×10^4 time steps with $\Delta t = 0.25$ ms. Time averages were computed after discarding a transient of 2×10^4 time steps. The results were averaged over 100 realizations. The arrow denotes the analytical estimate for M_c in the weak coupling limit. In the asynchronous regime, the average firing rate in the network changes from $f \approx 105$ Hz for $g_{\rm syn} = -0.1$ mV/ms to $f \approx 80$ Hz for $g_{\rm syn} = -0.6$ mV/ms.

Figure 10. The synchrony measure χ is plotted vs. the coupling strength $g_{\rm syn}$ for $M = 400$, $N = 800$ ($M_{\rm eff} = 800$). Parameters are: $T_r = 2$ ms, $\tau_1 = 1$ ms, $\tau_2 = 3$ ms, $N = 800$. Simulations were carried out with 4×10^4 time steps and $\Delta t = 0.25$ ms. A. No heterogeneity. Solid line: The external current is fixed at $I_{ext} = 1.816$ mV/ms. The firing rate decreases with increasing $-g_{\rm syn}$ from 100 Hz for $g_{\rm syn} = 0$ to 56 Hz for $g_{\rm syn} = -1$. Dotted line: The external current increases when $-g_{\rm syn}$ increases such that the average firing rate in the asynchronous state remains constant ($f = 100\ Hz$). B. Heterogeneity. the external current varies from neuron to neuron and is homogeneously distributed between $\bar{I}_{\rm ext} - \delta$ and $\bar{I}_{\rm ext} + \delta$. The average, $\bar{I}_{\rm ext}$, is determined such that the population average of the firing rate, f, in the asynchronous state is kept constant, $f = 100\ Hz$. Solid line: the width of the distribution is $\delta = 0.075$ mV/ms; The network activity is synchronized for $0.5\,{\rm mV/ms} \le -g_{\rm syn} \le 2.2\,{\rm mV/ms}$. Dotted line: the width of the distribution is $\delta = 0.15$ mV/ms. The network activity is always asynchronous. Simulations with larger N show that the residual non-zero value of χ are finite-size effects (result not shown). Simulations indicate that in the fully connected network with the same parameters, the asynchronous state becomes unstable at $-g_{\rm syn} \approx 0.6{\rm mV/ms}$ (result not shown).

Figure 11. The distribution histogram of the firing rates (A) and the coefficient of variation of the interspike distribution (B) for $M_{\rm eff} = 800$, and $N = 400, 800, 1600$. Parameters are: $T_r = 2$ ms, $\tau_1 = 1$ ms, $\tau_2 = 3$ ms, $f = 100$ Hz, $g_{\rm syn} = -25{\rm mV/ms}$. Simulations are done with 3.2×10^6

time steps and $\Delta t = 0.125$ ms. Results for $N = 400, 800, 1600$ are averaged over 40, 20, 10 realizations respectively and a bin width of 2 Hz. In both figures the silent neurons (neurons with firing rate < 2 Hz which are about 6.2% of the population) are not represented. In (B), the three curves superimpose almost perfectly and are hardly distinguishable.

Figure 12. A. The functions $J(y, 1)$ (solid line) and $(\pi/2)\, P(y, 1) \tan\alpha$ (dashed line) for $\alpha = -\pi/4$. B. A graph of the function $\beta(\alpha)$, referred to in Eq. 3.12 and defined in Eq. A.18, A.20.

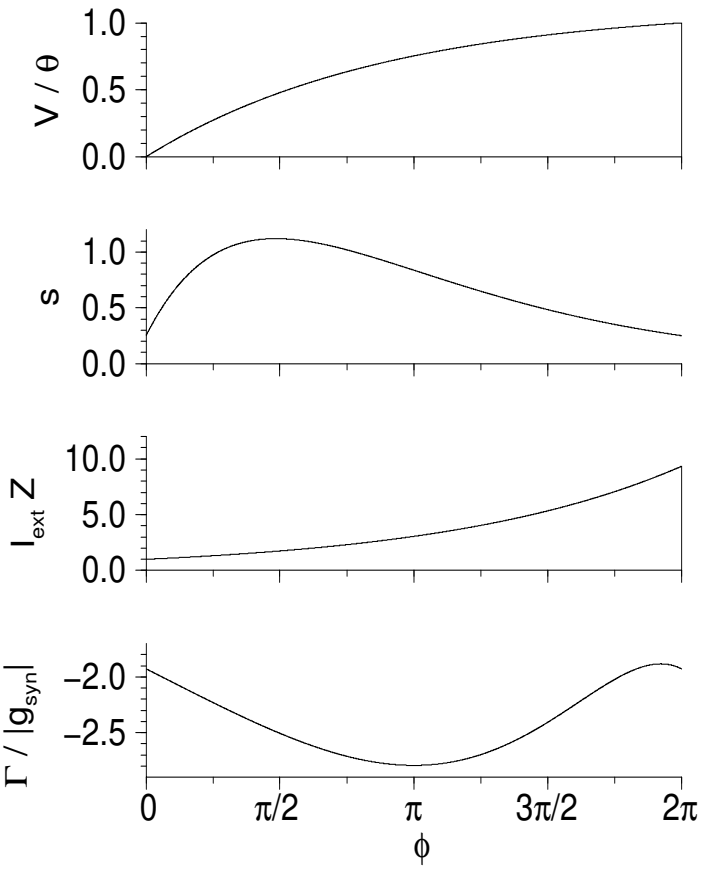

Fig. 1, Golomb, 2027

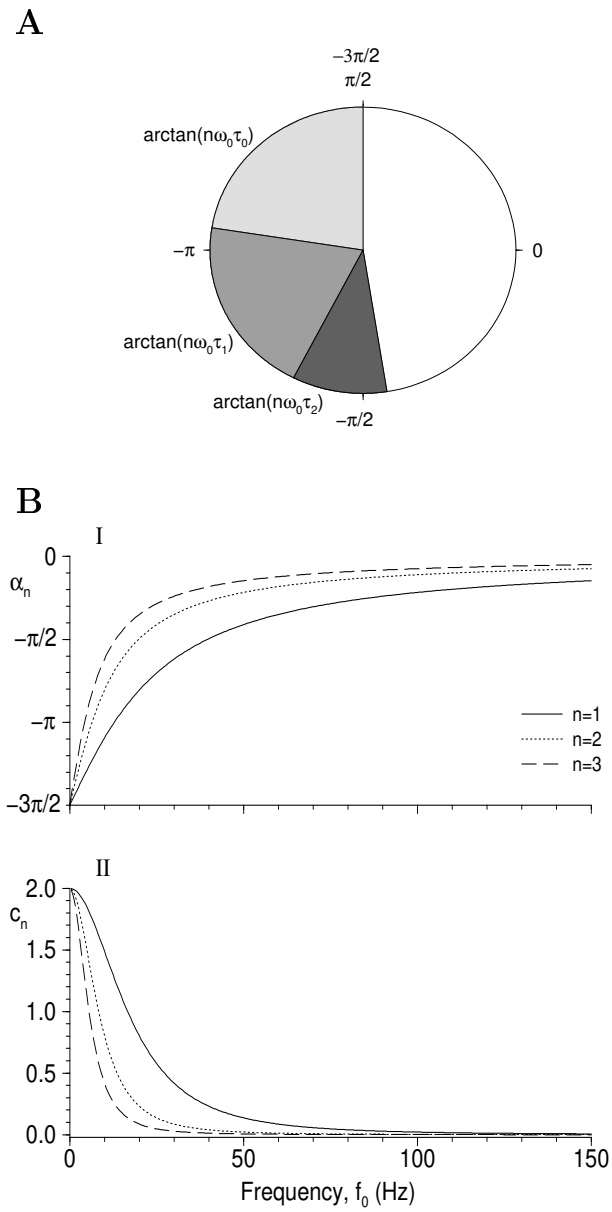

Fig. 2, Golomb, 2027

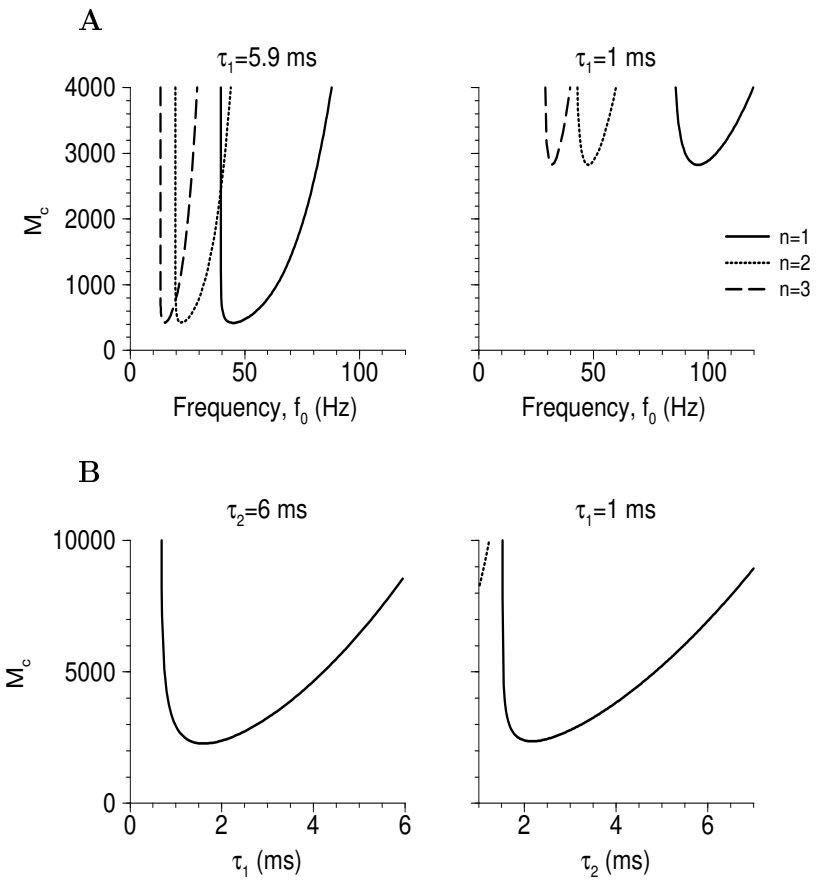

Fig. 3, Golomb, 2027

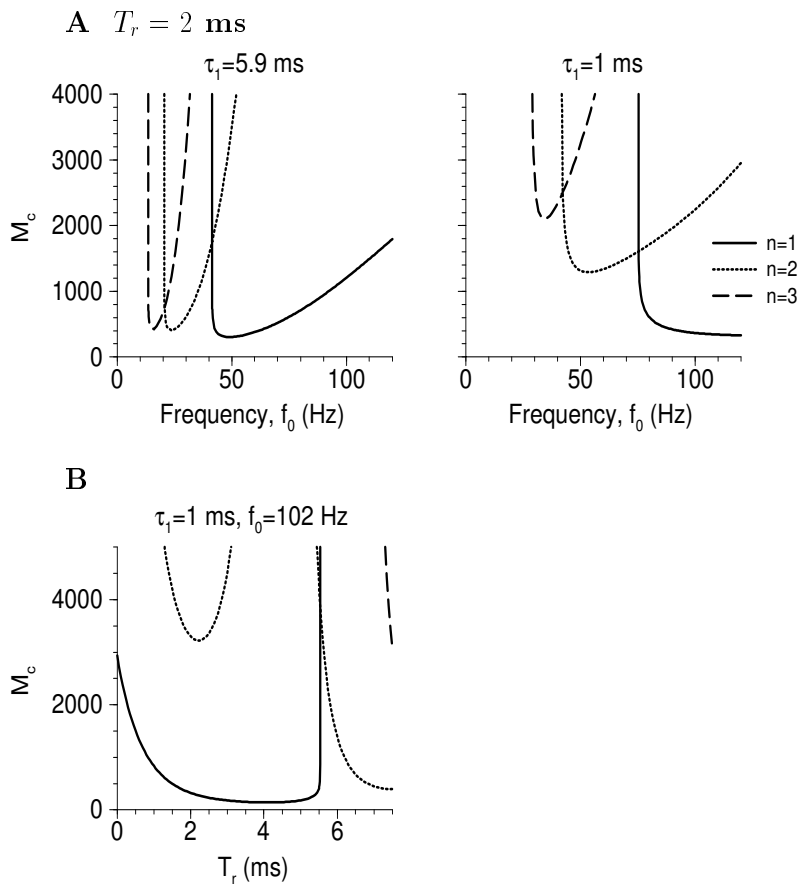

Fig. 4, Golomb, 2027

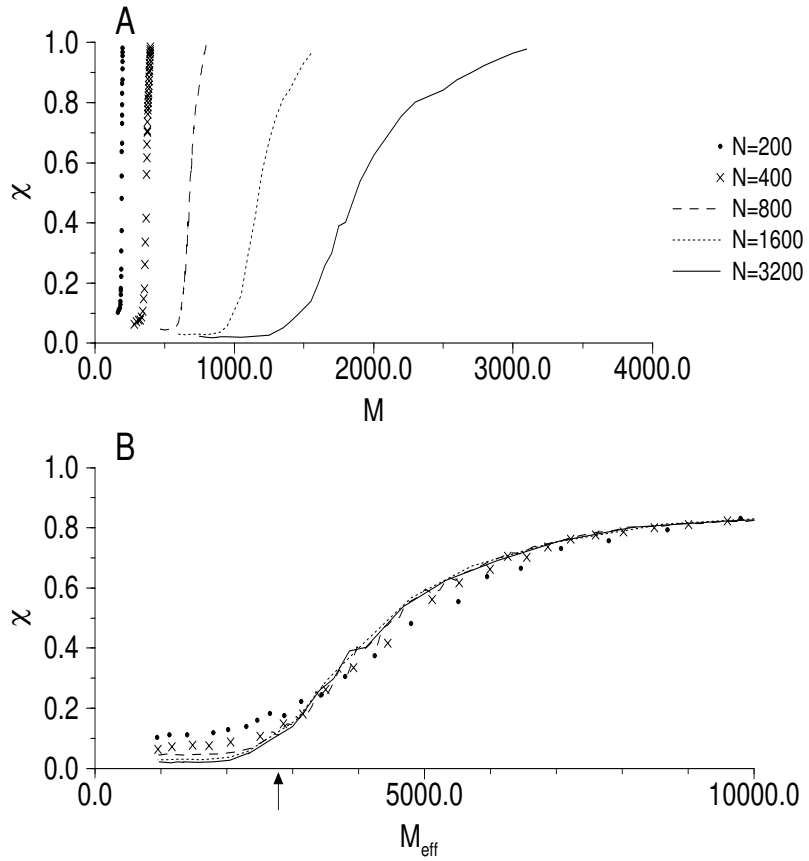

Fig. 5, Golomb, 2027

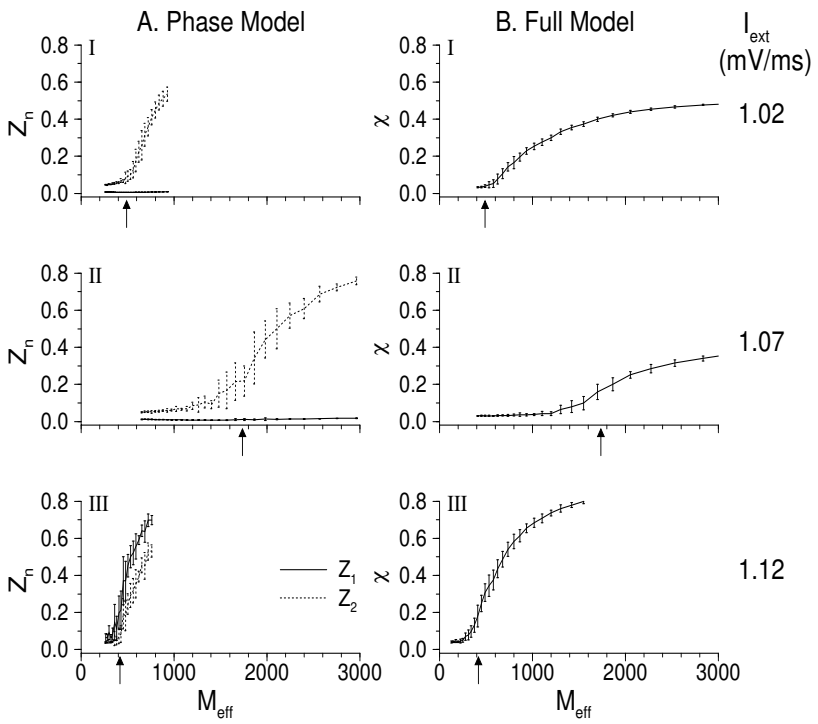

Fig. 6, Golomb, 2027

Fig. 7, Golomb, 2027

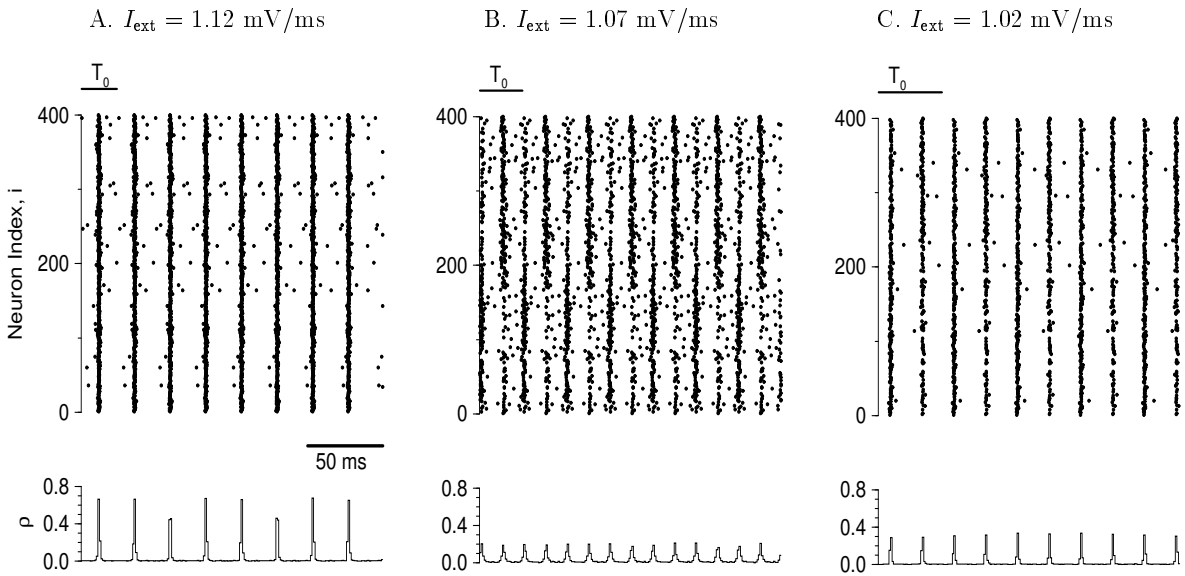

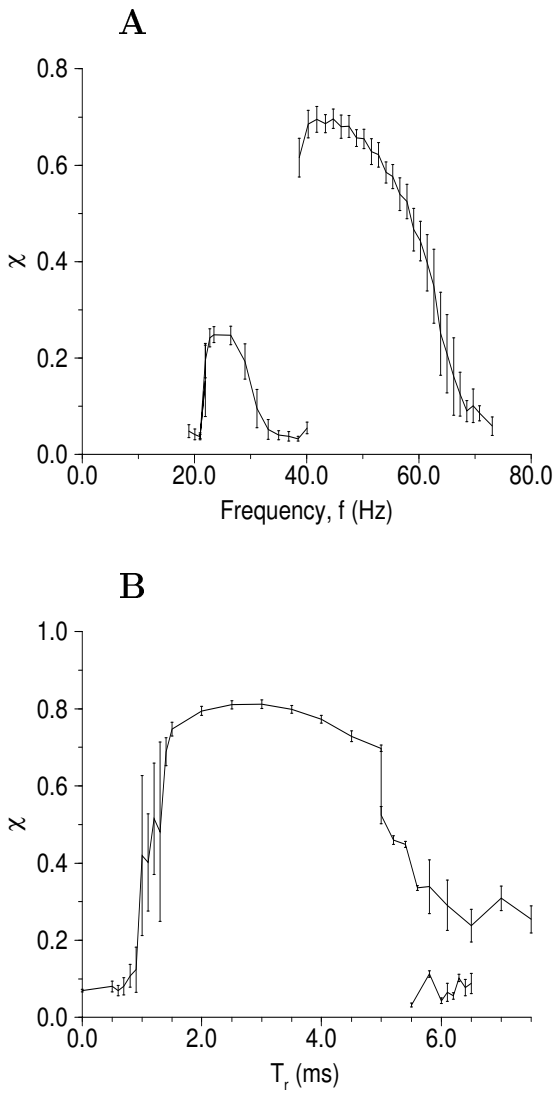

Fig. 8, Golomb, 2027

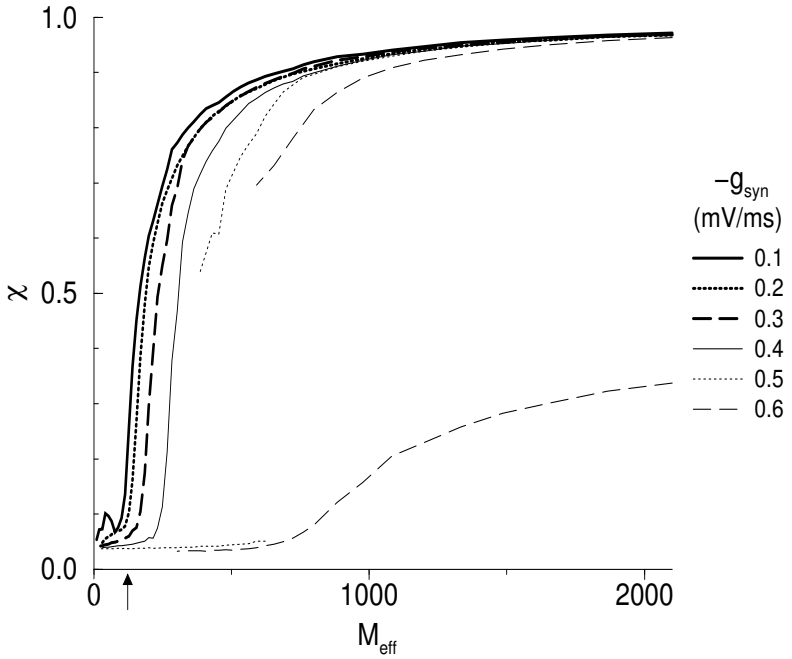

Fig 9, Golomb, 2027

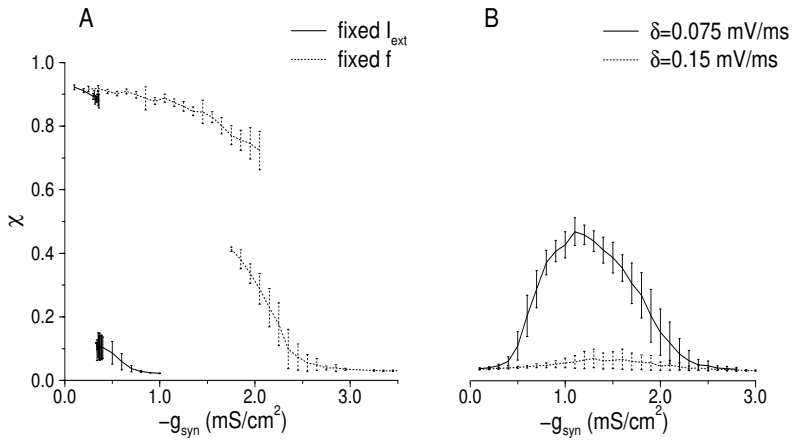

Fig. 10, Golomb, 2027

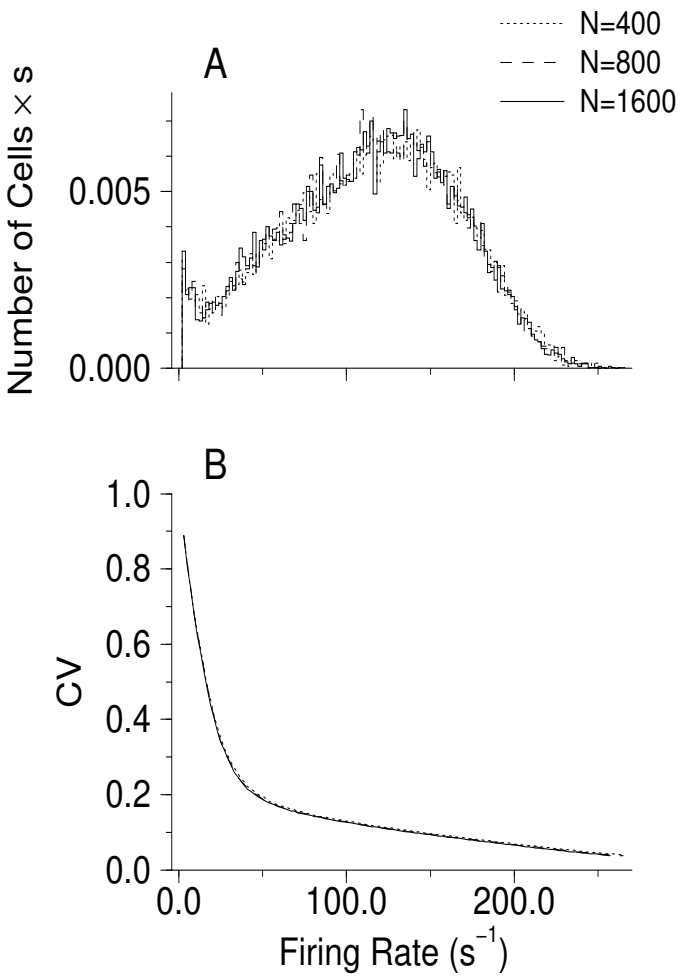

Fig. 11, Golomb, 2027

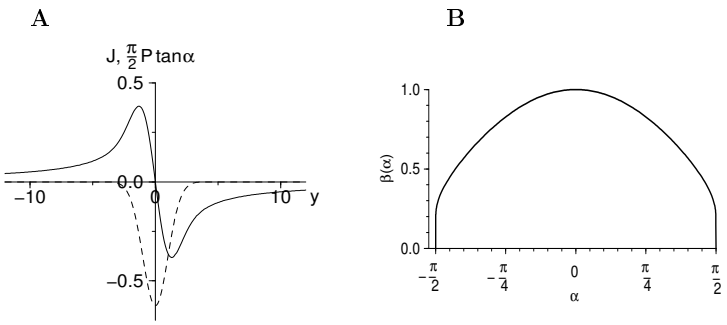

Fig. 12, Golomb, 2027